LIBRATIONAL DISPLACEMENTS OF SILICATE TETRAHEDRA IN RESPONSE TO TEMPERATURE AND PRESSURE

by

Robert T. Downs

Dissertation submitted to the Faculty of the
Virginia Polytechnic Institute and State University
in partial fulfillment of the requirements for the degree of
DOCTOR OF PHILOSOPHY
in
Geological Sciences

APPROVED:

G.V. Gibbs, Co-Chairman

M.B. Boisen, Jr., Co-Chairman

M.S.T. Bukowinski

P.H. Ribbe

C.T. Prewitt

December, 1992

Blacksburg, Virginia

LIBRATIONAL DISPLACEMENTS OF SILICATE TETRAHEDRA IN RESPONSE TO TEMPERATURE AND PRESSURE

by

Robert T. Downs

(Abstract)

Recently it has been concluded that the SiO_4 silicate tetrahedra in crystals behave as rigid bodies. This conclusion is based on analyses of the atomic displacement factors of Si and O atoms obtained from single crystal diffraction experiments wherein the amplitudes of atomic vibrations are ascribed to translational, librational and screw–correlated modes of motion for the entire SiO_4 group. If the displacement ellipsoids are considered to represent time averaged quadratic surfaces of equal configurational potential energy about the mean position of an atom, then an analysis of the these displacements should provide detailed information about the SiO_4 group and the crystal.

The apparent SiO bond lengths recorded for silicates over a range of temperatures are typically either invariant or exhibit a contraction with increasing temperature. A rigid-body thermal analysis was completed for the tetrahedra in nine silicates whose structures have been determined over a range of temperatures from 15 K to 1250 K and whose tetrahedra seem to behave as rigid units. The coordinates provided by the analysis yield bond lengths and polyhedral volumes corrected for the librational motion of each silicate tetrahedron. The bond lengths and volumes estimated for tetrahedra with four bridging oxygens seem to increase with temperature at a faster rate than those with four nonbridging oxygen atoms. Those for tetrahedra with two or three nonbridging oxygen atoms tend to increase at an intermediate rate. An analysis of the rigid-body motion of coordinated polyhedra yields a simple but accurate expression for correcting bond

lengths for thermal vibrations.

Observed anisotropic displacement parameters for Si and O atoms indicate that the SiO_4 tetrahedra in quartz behave as rigid bodies. A configurational potential energy curve, constructed from the librational components of the rigid body motion of the tetrahedra, shows a double well for α quartz and a single well for β quartz when plotted as a function of the displacement of the O atom with temperature. The configurational energetics of α and β quartz are examined with a theoretical potential energy function based on parameters obtained from molecular orbital calculations. The calculations indicate that the temperature behavior of α quartz is governed by the energetics of the SiOSi angle, in contrast to β quartz which is governed by the energetics of the SiO bond. The mechanism of the $\alpha \rightleftharpoons \beta$ transition is examined in terms of the experimental and modeled configurational potential energy curves. Evidence for the proposal that π bonding is the driving mechanism for the transition is lacking.

Structural and volume compressibility data for α–cristobalite were determined by single crystal X–ray diffraction methods for pressures up to ~1.6 GPa, where cristobalite undergoes a reversible phase transition. The bulk modulus was determined to be 11.5(7) GPa with a pressure derivative of 9(2). The SiOSi angle shows a greater decrease than observed for quartz and coesite while the SiO bond lengths and the OSiO angles remain essentially unchanged. The responses of V/V_0 and SiOSi angle to pressure for the silica polymorphs are compared and it is found that the percentage decrease in the volume is linearly correlated with the percentage decrease in the SiOSi angle, regardless of the framework structure type. A mathematical modeling of the energies of the structural changes that are induced by pressure suggests that the contribution to the total energy ascribed to SiOSi angle bending terms is the same in quartz and cristobalite.

Acknowledgements

The National Science Foundation is thanked for supporting this work with Grant EAR–8803933. Sharon Chiang drafted Figures 1–5 and 2–4. Her talents are much appreciated. Maryellen Cameron provided helpful insight into the experimental pitfalls of collecting and refining high temperature diffraction data.

The ideas for Chapter 2 found their roots in a stimulating discussion with Frank Hawthorne about the role of the thermal behavior of atoms when crystals were undergoing phase transitions. Professor Lee Johnson of the Mathematics Department at VPI&SU is appreciated for his work on the minimization algorithms in the MADMAX software.

The experimental work of Chapter 3 could not have been carried out without the kind patronage of Charlie Prewitt and a pre–doctoral fellowship at the Carnegie Institute of Washington's Geophysical Laboratory. I especially acknowledge the supervision and tutelage of Larry Finger and Bob Hazen. Most important, however, was the friendship developed with my co–worker, David Palmer, with whom the data were collected.

I came to Va Tech with a love for mineral collecting and I will be leaving with a love for minerals. There is no end to my gratitude to Jerry Gibbs for this. Jerry is the best. My undergraduate degree was in mathematics, so the link to mineralogy provided by Monte Boisen was invaluable. Paul Ribbe was always available for counsel and a chat. The year that Mark Bukowinski spent here was a very enjoyable year for me. I was able to talk with him about all sorts of things. In particular, his suggestion about taking the lattice dynamics courses was very good. My best friend ended up being the best guy to work with. Kurt Bartelmehs and I have both worked hard together and played hard together. I'm sorry to see these times draw to an end.

Meeting and marrying my sweetheart, Dori, was by far the smartest thing I have ever done. She has rounded the rough edges of my life. And, incidently, her father is a physicist. I am in debt to him for our weekly lunches and discussions, and for the instructions in lattice dynamics.

Finally, I am off to the Carnegie Institute of Washington's Geophysical Lab next month. I am extremely grateful for the four months I spent there last year. To have the opportunity of studying with Gibbs and then Prewitt is just too good to be true. I am a lucky guy.

Table of Contents

List of Figures

List of Tables

Chapter 1

Variations of Bond Lengths and Volumes of Silicate Tetrahedra with Temperature

Introduction

The atoms of a crystal are never at rest but are in perpetual oscillatory motion about their equilibrium positions with their mean square displacement amplitudes, MSDAs, increasing with temperature. A structural analysis of a crystal by diffraction methods can yield a set of precisely determined mean positional coordinates for each of its nonequivalent atoms, but, because of the oscillatory motions of the atoms, the separations calculated from these coordinates, referred to as the apparent interatomic separations, R, are always less than the mean interatomic separations, R_m (Cruickshank, 1956, 1961; Busing and Levy, 1964). It is these latter quantities that have chemical significance as they are the bonded and nonbonded mean interatomic separations that obtain between atoms at their equilibrium positions.

As observed by Busing and Levy (1964), before an estimate can be made of the mean interatomic separation between a pair of atoms, a knowledge is required of the correlations that obtain among the respective motions of these atoms. Unfortunately, of the possible correlated motions, only a few are sufficiently well understood so that a mean interatomic separation can be accurately estimated. One such motion is the rigid-body motion often exhibited by the atoms of a molecule that are strongly linked together and that exhibit both translational and librational (rotatory) modes of oscillations (Cruickshank, 1957; Willis and Pryor, 1975). Accurate estimates of the mean interatomic separations for such a rigid molecule can be obtained from a TLS (Translational, Librational and Screw modes of motion) modeling of the thermal motion (Cruickshank, 1957; Schomaker

and Trueblood, 1968). Not only do the separations calculated from the atomic coordinates determined for molecular crystals provided by the analysis tend to be in better agreement with those obtained by spectroscopic methods (Dunitz et al. 1988), but also the lengths of bonds that have similar strengths tend to show a relatively narrow range of values.

In recent studies of the MSDAs observed for the Si and O atoms in a number of ordered framework silicate minerals, Bürgi (1989), Downs (1989), Downs et al. (1990) and Armbruster et al. (1990) claim that the coordinated silicate tetrahedra in these minerals seem to behave as rigid bodies. These studies indicate that the Si and O atoms move in tandem along each SiO bond so that the MSDA of Si toward O, z^2_{SiO}, tends to equal that of O toward Si, z^2_{OSi}. Downs et al. (1990) inferred from this result that the SiO bonds in these structures are oscillating back and forth as rigid units. Similar results seem to hold for the nonbonded OO separations that define the edges of each SiO_4 group. Furthermore, as one might expect, the MSDAs along the line of separation between a given pair of oxygens in adjacent silicate tetrahedra are not, in general, equal. Based on these observations, the tetrahedra in ordered framework silicates seem to behave as rigid bodies (with fixed interatomic separations) librating and translating back and forth about their equilibrium positions.

In this study, a TLS rigid-body thermal motion modeling is completed for the SiO_4 silicate tetrahedra in nine selected ordered silicates whose diffraction data were recorded over a relatively wide range of temperatures. Estimates of the mean interatomic SiO separations, R_{TLS}(SiO), calculated from the coordinates obtained in the TLS analysis yield separations for room temperature structure determinations that are typically about 0.005Å longer than R(SiO), the observed apparent SiO bond length. In addition, R_{TLS}(SiO) calculated for data recorded

at temperatures up to 1250K are considerably greater, as much as 0.03Å, than R(SiO). In fact, R_{TLS}(SiO) increases or is unchanged with temperature while R(SiO) typically decreases or remains unchanged with increasing temperature. As a TLS analysis involves a tedious calculation, a simple expression, referred to as the simple rigid bond correction, was derived to estimate the mean interatomic separations for rigid coordinated polyhedra. Application of this correction to the nine selected silicates yields bond lengths that match those obtained in a TLS analysis with an esd of 0.002Å.

A Review of Bond Length Correction Expressions

In a careful study of bond length errors ascribed to the libration of a molecule in a molecular crystal, Cruickshank (1956) showed that the positional error of an atom, Δr, in a radial direction can be estimated by

$$\Delta r = \frac{1}{2r}\left(\frac{s^2}{1 + s^2/q^2} + \frac{t^2}{1 + t^2/q^2}\right), \qquad (1\text{-}1)$$

where r is the distance between the libration center of the molecule and the atom, s^2 and t^2 represent the librational MSDAs of the atom perpendicular to the radial direction, and where q^2 represents a spherical Gaussian breadth parameter fit to the electron density peak of the atom that measures translational motion only. Inasmuch as q^2, s^2 and t^2 are difficult to obtain, this equation has not found wide application. In the derivation of Equation 1–1, it was assumed that only the librations perpendicular to the radial direction are relevant, an assumption that is known to hold for molecules with $\bar{1}$, $\bar{3}$, $\bar{6}$ or $\bar{4}3m$ point symmetry (Johnson, 1969a). By relaxing this assumption, Cruickshank was able to express the rigid-body motion of a molecule in a more general way in terms of two symmetric tensors, one representing the librational component, L, of the rigid-body motion and the other, T, the translational component. Since translational motion does

not affect bond lengths, the librational component can be isolated and used in the expression

$$[\Delta \mathbf{v}]_C = \frac{1}{2}[(\text{trace}L)I_3 - L][\mathbf{v}]_C, \tag{1-2}$$

to correct the Cartesian coordinates, $[\mathbf{v}]_C$, of the atoms. This expression is based on the assumption that the librational oscillations are not too large ($< 10 - 15°$). However, Cruickshank's model did not take into account any correlation between translational and librational modes of motion, which subsequently was denoted the screw mode of motion by Schomaker and Trueblood, (1968). When the rigid-body parameters of a molecule are obtained in a refinement involving translational, librational and screw motion, the elements of the resulting L matrix can be used, as defined by Equation 1–2, to provide thermally corrected positional coordinates for atoms in rigid molecules. Bond lengths, R_{TLS}, calculated from these coordinates have proven to be accurate estimates of the mean separations among the atoms in molecular crystals (Dunitz et al. 1988). To our knowledge, this procedure is the most accurate method known to date for estimating R_m in rigid molecules.

Perhaps the most widely used expression for correcting bond length is provided by the Busing and Levy, (1964) 'riding model' where one of the atoms, Y, is assumed to be strongly linked to one much heavier atom, X, upon which it appears to 'ride'. This model is based on the assumption "that atom Y has all of the translational motion of atom X plus an additional motion uncorrelated with the instantaneous position of atom X" (Johnson, 1969b). An estimate of R_m for a pair of atoms exhibiting riding motion is given by

$$R_{rid} = R + \frac{\overline{w}_Y^2 - \overline{w}_X^2}{2R}, \tag{1-3}$$

where $\overline{w}_X^2$ and $\overline{w}_Y^2$ are the average MSDAs of atoms X and Y in the plane perpendicular to the XY bond. The widespread use of the riding model may be ascribed

to the relative ease with which the $\overline{w}^2$-values can be obtained and to its success in obtaining reasonable OH bond length corrections.

Thermal Expansion of Silicate Tetrahedra

The apparent SiO bond lengths, R(SiO), recorded for a number of silicate minerals over a variety of temperatures, typically are either invariant or show a slight contraction with increasing temperature. As an illustration of this point, the thermal expansion rates of R(SiO), as defined by the slopes of the regression lines fit to R(SiO) as a function of T, are presented in Table 1–1 for low albite, acmite, diopside, jadeite, and spodumene, Na fluor-richterite and K fluor-richterite, andalusite and kyanite (Smith et al. 1986; Harlow and Brown, 1980; Armbruster et al. 1990; Winter et al. 1977; Clark et al. 1969; Cameron et al. 1973; Levien and Prewitt, 1981; Cameron et al. 1983; Winter and Ghose, 1979). These minerals were chosen because the z^2_{OSi} and z^2_{SiO} values of their their SiO bonds are highly correlated with $z^2_{OSi} \approx z^2_{SiO}$, satisfying the criteria set forth by Downs et al. (1990). Also, the MSDA's of the O atoms, calculated along the edges of the tetrahedra, tend to be equal except at the highest temperatures. Taken together, these results indicate that the SiO_4 tetrahedra in these structures behave as rigid bodies, except at the high temperatures, where the rigid model may be expected to fail.

An examination of the expansion rates for the bonds in low albite and in Na and K fluor-richterite indicates that they contract for the most part with increasing temperature. The rates recorded for the remaining silicates are marginally positive or zero. In a discussion of the implications of these results, Winter et al. (1977) noted that the invariant behavior of the SiO bond length with increasing temperature requires that the potential well for the bond be quadratic in nature. They also observed that the contraction of the bond with increasing

temperature requires that the cubic term characterizing the anharmonicity of the well be positive in sign. This implies that the curvature of the well increases more slowly at shorter bond lengths than it does at longer bond lengths, relative to the equilibrium bond length. Winter et al. (1977) considered both interpretations of the shape of the potential well to be unreasonable. In an attempt to resolve this problem, they corrected R(SiO) and R(AlO) in low albite for thermal motion, using the four equations presented by Busing and Levy, (1964). These equations yield four sets of corrected bond lengths that show a range of values that differ by as much as 0.03Å. Inasmuch as the correlated motions of the atoms in low albite were unknown, they were unable to decide which set of corrected bond lengths provides an accurate estimate of the mean bond lengths in the mineral.

As discussed earlier, recent studies of the temperature factors for the Si, Al and O atoms of the framework silicates, including low albite, indicate that their tetrahedra behave as rigid bodies. Using the strategies employed by Downs et al. (1990) for the framework silicates, similar calculations were completed for the silicates in Table 1–1. As the trends between the MSDAs for the SiO bonds and OO separations are the same as those recorded for ordered frameworks , it is concluded that the tetrahedra in these silicates also behave as rigid bodies. Therefore, a TLS analysis was completed for each silicate group to obtain an L-tensor, using a FORTRAN77 program written for this purpose. With Equation 1–2, the thermally corrected coordinates of the atoms for each tetrahedron were estimated and R_{TLS}(SiO) was calculated for each bond.

Using these estimates of the mean SiO bond lengths, expansion rates for R_{TLS}(SiO) were calculated and are presented in Table 1–1 where it is seen that almost all of the bonds expand with increasing temperature. Figure 1–1 compares the variation with temperature of the apparent $Si_{1m}O_{bm}$ bond length in low albite

with that of the TLS estimate of the mean bond length. This plot shows that the TLS corrected bond length is appreciably longer, ~ 0.03Å, than the apparent length of the bond at 1200 K. As the expansion rates of all the TLS corrected SiO bond lengths in low albite are similar to that of the $Si_{1m}O_{bm}$ bond, it is concluded that the SiO bond lengths in low albite expand, as expected, with increasing temperature.

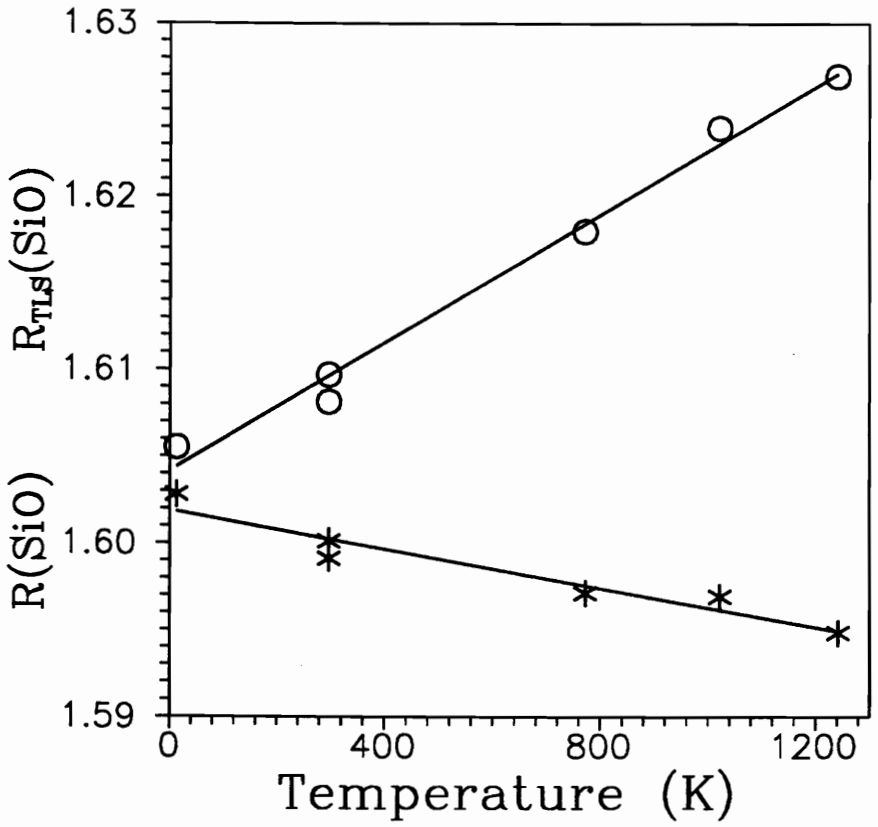

Figure 1–1. A scatter diagram of the variation of the SiO bond length with temperature for the $Si_{1m}O_{Bm}$ bond in low albite. The uncorrected, apparent bond lengths, R(SiO), are plotted as asterisks, while the TLS bond lengths, R_{TLS}(SiO), corrected for rigid-body libration, are plotted as open circles. Note that the uncorrected bond lengths appear to shorten with increasing temperature, however, when corrected, the bonds increase in length.

In a study of the high temperature crystal chemistry of single chain silicates, Cameron et al. (1973) suggested that the bridging SiO bond lengths, R(SiO_{br}),

in these minerals tend to expand at a faster rate than the nonbridging ones, R(SiO_{nbr}). The data in Table 1–1 seem to support this claim. For example, the average expansion rate of the bridging SiO_{br} bonds, $< \partial R_{TLS}(SiO_{br})/\partial T >$, for the single chain silicates, 10.5×10^{-6}Å/K, is significantly larger than that, 7.8×10^{-6}Å/K, calculated for $R_{TLS}(SiO_{nbr})$. In addition, $< \partial R_{TLS}(SiO_{br})/\partial T >$ calculated for low albite, which only contains O_{br}, is larger, 12.6×10^{-6}Å/K, than $< \partial R_{TLS}(SiO_{nbr})/\partial T >$, 6.0×10^{-6}Å/K, calculated for andalusite and kyanite which only contain O_{nbr}. There appears to be two families of expansion rates with $R_{TLS}(SiO_{br})$ expanding at nearly twice the rate of $R_{TLS}(SiO_{nbr})$.

With the coordinates obtained from the TLS modeling, volumes were calculated for each of the silicate tetrahedra in the nine silicates. In an examination of the variation of these volumes, V_{TLS}, with temperature, linear regression analyses were completed for V_{TLS} as a function of T. The resulting expansion rates for these tetrahedra are given in Table 1–1. The correlations between V_{TLS} and T were found to be better developed than those between R_{TLS}(SiO) and T. The overall average expansion rate of V_{TLS} is 35×10^{-6}Å^3/K, a value that is significantly larger than the zero value reported by Hazen and Finger (1982), and corroborated with our nine silicates, for the silicate tetrahedra uncorrected for thermal motion. As observed above, $R_{TLS}(SiO_{br})$ increases, in general, at a faster rate with temperature than does $R_{TLS}(SiO_{nbr})$. Therefore, it is not surprising that the silicate tetrahedra in low albite, where each tetrahedron consists of four O_{br}, expand at about twice the rate as they do in kyanite and andalusite, where each tetrahedron consists of four O_{nbr}. The tetrahedral volumes for the single and double chain silicates, where the tetrahedra contain two or three O_{br}, expand at an intermediate rate. Like Cameron et al. (1973), no explanation is currently offered as to why SiO bridging bonds expand at a faster rate than nonbridging ones.

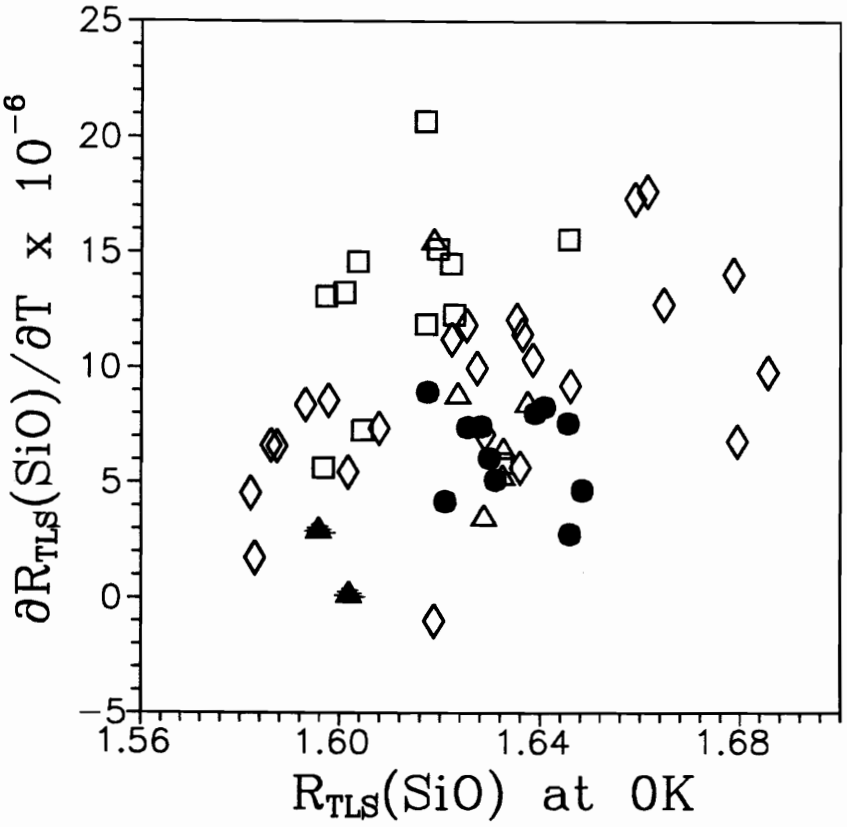

Figure 1–2. A scatter diagram of the slope versus intercept for R_{TLS}(SiO), indicating that the expansion rates of mean SiO bonds do not seem to depend on bond length. The low albite tetrahedral data, with four O_{br}, are plotted as squares, the chain silicates, with three and two O_{br}, are plotted as triangles and diamonds, respectively, and the orthosilicates, with no O_{br}, are plotted as circles. The open symbols indicate bridging bonds while the closed ones indicate nonbridging bonds. Note that the bridging bonds tend to have larger expansion rates than the nonbridging ones.

In a study of the thermal expansion and high temperature crystal chemistry of the Al_2SiO_5 polymorphs, Winter and Ghose, (1979) argue that longer bonds should show a greater increase in length with increasing temperature than shorter ones because the latter are usually stronger (See also Megaw, 1971; Hazen and Prewitt, 1977). This argument not only seems to hold for the values of R(SiO) recorded for these aluminosilicates, but it also seems to hold for silicates in general (Hazen and Finger, 1982). However, Figure 1–2 shows for the nine silicate studied

that the expansion rate of SiO seems to be independent of R_{TLS}(SiO). It also shows that the expansion rate of an SiO bond seems to be related to whether the bond involves a bridging or nonbridging O atom with bridging bonds tending to expand at faster rates than nonbridging ones. On the other hand, the expansion rates of the tetrahedral volumes seem to depend on V_{TLS}, with the volumes of the smaller tetrahedra in low albite increasing at a faster rate than those of the larger tetrahedra in the remaining eight silicates (Figure 1–3). As the linkages of the tetrahedra in low albite are different from those in chain and orthosilicates, it appears that the expansion rates also depend on the tetrahedral linkage, with expansion rates increasing with the number of bridging O atoms. This is contrary to the suggestion of Hazen and Finger (1982) that each coordinated polyhedron has a unique volume expansion coefficient.

A Simple Rigid Bond Model Correction

It is an extensive undertaking to calculate the L-matrix that is required to correct the SiO bond length for thermal motion effects, using Equation 1–2. Consequently, a simpler expression for correcting rigid bond lengths in coordinated polyhedra will be derived that uses the isotropic rather than the anisotropic temperature factors of the atoms that comprise the polyhedra. The necessary and sufficient conditions that must hold for this simple rigid bond (SRB) correction are as follows: (1) The bonds must be appear to be rigid and (2) the coordinated cation only exhibits translational motion with little or no librational motion.

If the bonds of a coordinated polyhedron, XY_n, appear to be rigid, then the interatomic separation between the central cation, X, and each of its coordinated anions, Y, will tend to remain fixed. This implies that the MSDAs of the X and Y atoms will tend to be equal along an XY bond, $z^2_{XY} = z^2_{YX}$, (Hirshfeld, 1976; Dunitz et al. 1988). In particular, Downs et al. (1990) have shown that

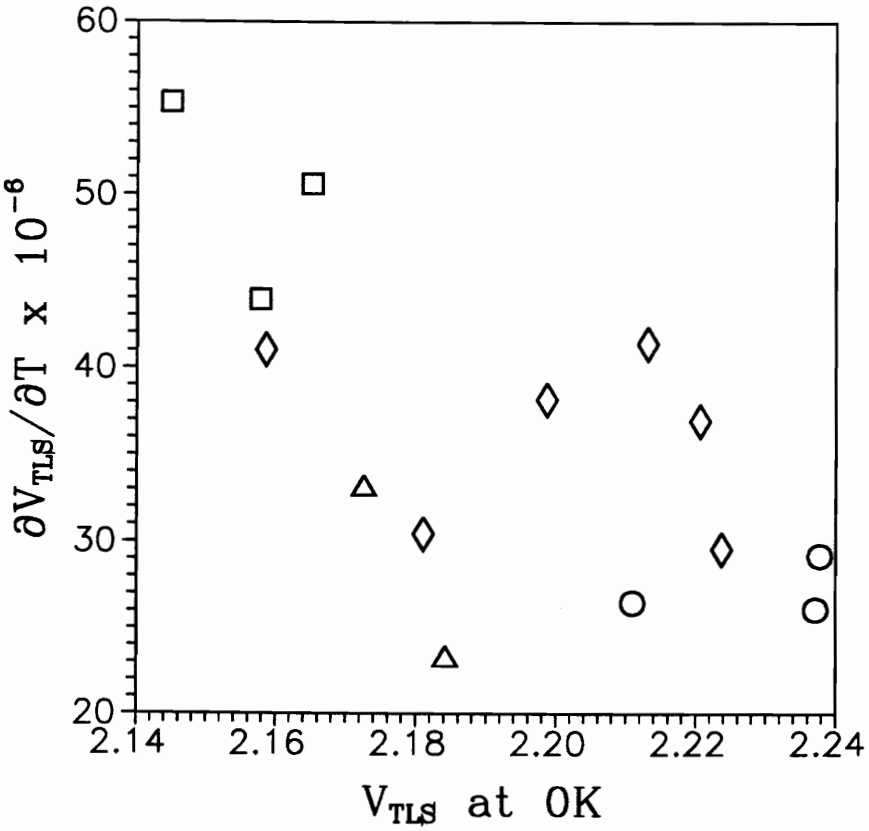

Figure 1–3. A scatter diagram of the slope versus intercept for $V_{TLS}(SiO_4)$. The low albite tetrahedral data, with four O_{br}, are plotted as squares, the chain silicates, with three and two O_{br}, are plotted as triangles and diamonds, respectively, and the orthosilicates, with no O_{br}, are plotted as circles. The distribution of these data suggests that expansion rate of V_{TLS} depends on the magnitude of V_{TLS}, which represents the mean volume of the tetrahedra, at 0 K.

this condition seems to hold for the SiO bonds in a large number of ordered framework silicates. More than 400 other silicate structures have been examined and this condition seems to hold for the SiO bonds in the great majority of these structures.

If the second condition is satisfied, then the axes of libration of the coordinated polyhedron lie near the central cation. When this is the case, the T matrix, obtained from the TLS fit, should match the temperature factor matrix of the

cation within its experimental errors. All the framework structures examined by Downs et al. (1990) and all the silicates examined in this paper, including the great majority of the other 400 silicate structures mentioned above, exhibit this property. This condition is demonstrated in Figure 1–4 where the isotropic equivalent of the translational motion of a silicate group, $T_{eq}(SiO_4)$, is seen to be highly correlated with the isotropic equivalent temperature factor of the central Si atom, $B_{eq}(Si)$. In this case, $T_{eq}(SiO_4)$ is calculated using the same formalism that is used to calculate $B_{eq}(Si)$. Interestingly, the six-coordinated polyhedra in many of these silicates conform with this condition as well.

Suppose that: (1) the center of libration of the XY_n coordinated polyhedron is located at the central X atom, and (2) suppose that L_1^2 and L_2^2 are the MSDAs of the Y–atom, ascribed to its libration, projected onto the axes X_1 and X_2. Figure 1–5 shows a set of Cartesian coordinate axes, $\{X_1, X_2, X_3\}$, where X_3 is chosen to parallel one of the XY bonds in the polyhedron and X_1 and X_2 are chosen to be perpendicular to the bond. The MSDA of libration projected onto a plane perpendicular to the bond is given by $L_1^2 + L_2^2$, and so by the Pythagorean rule

$$R_{SRB}^2 = R^2 + L_1^2 + L_2^2.$$

If assumption (2) is satisfied, then

$$L_1^2 + L_2^2 = \sigma_{1,Y}^2 - \sigma_{1,X}^2 + \sigma_{2,Y}^2 - \sigma_{2,X}^2,$$

where $\sigma_{i,X}^2$ and $\sigma_{i,Y}^2$ are the MSDAs of atoms X and Y projected onto the X_i^{th} axis. If condition (1) is satisfied, i.e., $z_{YX}^2 = z_{XY}^2$, then

$$\begin{aligned} R_{SRB}^2 &= R^2 + (z_{YX}^2 + \sigma_{1,Y}^2 + \sigma_{2,Y}^2) - (z_{XY}^2 + \sigma_{1,X}^2 + \sigma_{2,X}^2) \\ &= R^2 + \frac{3}{8\pi^2}(B_{eq}(Y) - B_{eq}(X)), \end{aligned} \tag{1-4}$$

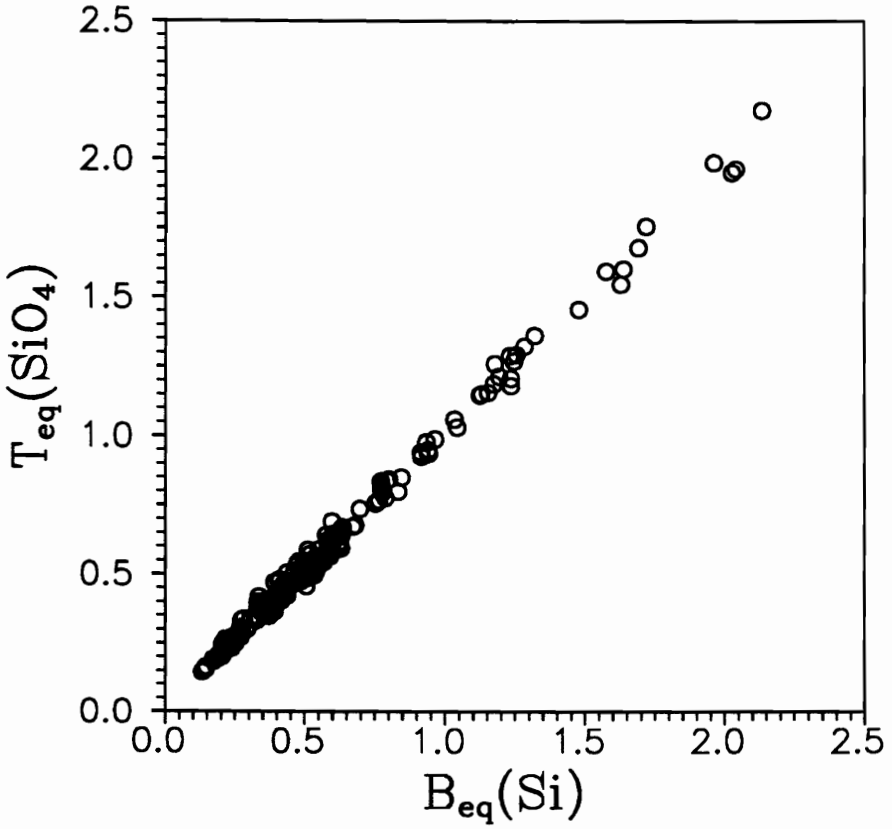

Figure 1–4. A scatter diagram of the equivalent isotropic temperature factor for the Si atom, B_{eq}(Si), against the derived equivalent isotropic translational motion parameter, $T_{eq}(SiO_4)$. The Pearson correlation coefficient is 0.997. This plot indicates that the thermal motion of the Si atom can be considered to be translational only and that there is essentially no librational component to its motion.

where B_{eq} is the isotropic equivalent temperature factor. It is noteworthy that when the two conditions hold, $\overline{w}_Y^2 - \overline{w}_X^2$ must equal $L_1^2 + L_2^2$. This implies that the 'riding model' defined by Equation 1–3 provides a good estimate of the mean bond lengths for rigid coordinated polyhedra.

Boisen et al. (1990) found that R(SiO) correlates well with B(O)-B(Si). This correlation is given a theoretical basis by Equation 1–4. In fact, it can be shown that the regression coefficient for R(SiO) vs. B(O) should be $\sim 3/(32R\pi^2) = 0.0059$ if it is assumed that B(Si)$\sim 1/2B$(O). The regression coefficient obtained

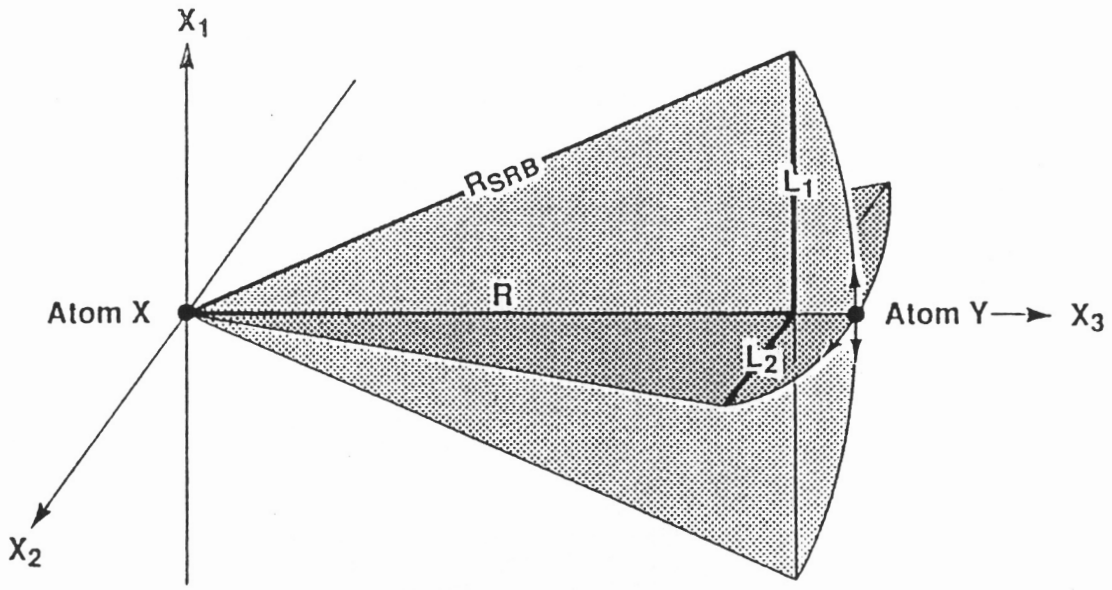

Figure 1–5. Librational motion of an XY bond in a XY_n rigid coordinated polyhedron, modified after Willis and Pryor (1975). R_{SRB} denotes an XY bond corrected for simple rigid bond motion, R is the apparent XY bond length, L_1 and L_2 denote the rms displacement amplitude of atom Y ascribed to the librational motion of the XY_n coordinated polyhedron projected on a plane perpendicular to R.

by Boisen et al. (1990) for the silica polymorphs and the clathrasils is ~ 0.006, matching the theoretical value given above.

The simple rigid bond model, as observed above, indicates that the isotropic temperature factors of the anions comprising a rigid coordinated polyhedron should be significantly larger than that of the coordinated cation, regardless of the masses of the atoms, because the temperature factors of the anions embody all of the translational motion of the cation plus the librational motion of the coordinated polyhedron. This observation is supported, for example, by a structural

analysis of SiS_2 (Prewitt and Young, 1965) which shows that the isotropic temperature factors of the S atoms comprising the rigid SiS_4 tetrahedra are significantly larger, $B_{iso}(S)=1.3Å^2$, than that observed for Si, $B_{iso}(Si)=0.7Å^2$, despite the fact that the mass of a S atom is about 15% larger than that of Si. A similar observation can be made for the rigid $SiSe_4$ tetrahedra in $SiSe_2$: the $B_{iso}-$value for Se is observed to be significantly larger ($2.7Å^2$) than the $B_{iso}-$value observed ($2.1Å^2$) for Si (Peters and Krebs, 1982), despite the larger mass of Se. If the temperature factors of these anions were smaller than that of Si, then Equation 1–4 would predict that the corrected bond length would be shorter than observed which contradicts Busing and Levy's assertion that thermally corrected bond lengths must always be longer than uncorrected ones. If the predictions of this model are correct, then a refined structure may be viewed as suspect and unsuitable for a crystal chemical study of bond length and angle variations (Boisen et al. 1990) when the B–values of a cation in a rigid coordinated polyhedron are significantly larger than the B–values of the coordinating anions.

As shown in Figure 1–6, R_{SRB}(SiO) is highly correlated with R_{TLS}(SiO) with a Pearson correlation of 0.996 and a slope and intercept of 1.0 and 0.0, respectively. More than 210 of the 244 SRB corrected bonds lengths agree to within 0.002Å of the TLS corrected values. The ones that depart from the regression line were recorded in high temperature structural analyses, where the rigid model may be breaking down and OSiO angle bending modes may be activated (Megaw, 1973). Figure 1–6 demonstrates that the simple rigid bond correction is a good estimator of the mean bond lengths for a coordinated polyhedron exhibiting rigid bond motion. The expansion rates of both the bond lengths and the tetrahedral volumes provided by the SRB corrections are statistically identical with those provided by a TLS correction.

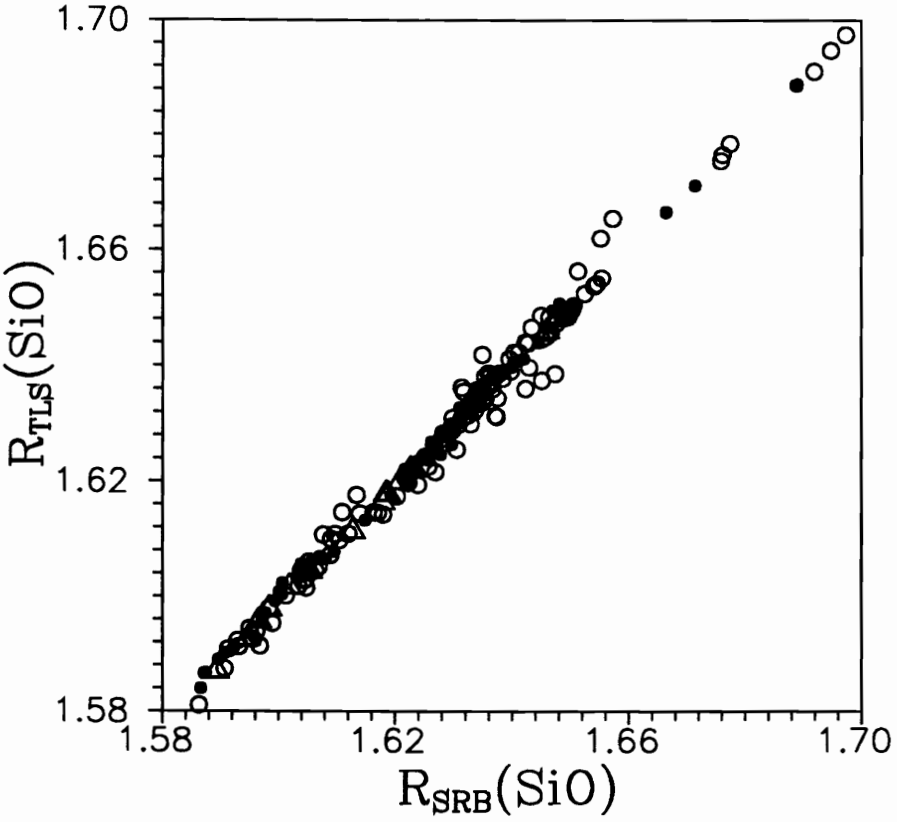

Figure 1–6. A scatter diagram of R_{SRB}(SiO) vs. R_{TLS}(SiO). The Pearson correlation coefficient is 99.6%, with 86% of the SRB corrected bond lengths being within 0.002Å of the *TLS* corrected bond lengths. Open triangles represent bond length data recorded at low temperature, solid circles represent data recorded at room temperature and open circles represent data recorded at high temperatures.

Conclusions

A *TLS* analysis was completed in this study on the silicate tetrahedra in nine silicates whose structures were determined over a range of temperatures from 15K to 1250 K. The analysis yields bond lengths for the silicate structures determined at room temperature that are slightly longer (~0.005Å) than the uncorrected ones. On the other hand, the analysis yields bond length data for the structures determined at high temperatures that exceed the uncorrected bond lengths by as much as 0.03Å. The libration angles calculated for the silicates examined in

this study were all less than 12° . Our analysis of the systematic errors due to the correction of bond lengths by the TLS method indicates that the maximum error in the resulting bond lengths is no more than ~0.001Å which is well within the estimated error. Furthermore, it is found that corrected bond lengths almost always increase in a regular way with increasing temperature.

Table 1–1. Linear Regression Slopes ($\times 10^{-6}$) for R(SiO), R_{TLS}(SiO), V(SiO_4) and V_{TLS}(SiO_4) as a Function of Temperature (K)

	R(SiO) (Å/K)	R_{TLS}(SiO) (Å/K)	V(SiO_4) (Å^3/K)	V_{TLS}(SiO_4) (Å^3/K)
albite				
$Si_{1m}O_{a1}$	−5(1)	13(1)	−17(2)	55(3)
$Si_{1m}O_{bm}$	−6(1)	15(1)		
$Si_{1m}O_{cm}$	−3(1)	12(1)		
$Si_{1m}O_{dm}$	−2(1)	15(1)		
$Si_{2o}O_{a2}$	−7(2)	6(2)	−14(2)	44(1)
$Si_{2o}O_{bo}$	−10(2)	6(2)		
$Si_{2o}O_{cm}$	6(1)	21(1)		
$Si_{2o}O_{dm}$	−3(1)	12(1)		
$Si_{2m}O_{a2}$	2(1)	16(1)	−10(1)	51(2)
$Si_{2m}O_{bm}$	−2(1)	15(2)		
$Si_{2m}O_{co}$	−1(1)	13(1)		
$Si_{2m}O_{do}$	−8(1)	7(1)		
acmite				
SiO1	5(2)	10(1)	10(2)	38(3)
SiO2	0(1)	9(1)		
SiO3a	5(4)	12(4)		
SiO3b	2(2)	9(2)		
diopside				
SiO1	0(2)	5(2)	7(4)	37(4)
SiO2	−2(2)	7(2)		
SiO3a	5(3)	13(3)		
SiO3b	3(1)	10(1)		
jadeite				
SiO1	2(1)	6(2)	7(2)	30(3)
SiO2	2(2)	8(2)		
SiO3a	1(1)	7(1)		
SiO3b	5(2)	10(3)		
spodumene				
SiO1	6(2)	11(2)	5(4)	41(3)
SiO2	−4(1)	7(1)		
SiO3a	1(1)	11(1)		
SiO3b	2(1)	12(1)		

Table 1–1.(cont.) Linear Regression Slopes ($\times 10^{-6}$) for R(SiO), R_{TLS}(SiO), $V(SiO_4)$ and $V_{TLS}(SiO_4)$ as a Function of Temperature (K)

	R(SiO) (Å/K)	R_{TLS}(SiO) (Å/K)	$V(SiO_4)$ (Å^3/K)	$V_{TLS}(SiO_4)$ (Å^3/K)
Na Fluor-Richterite				
Si1O1	−4(2)	0(1)	−11(5)	23(3)
Si1O5	−6(1)	4(2)		
Si1O6	−0(3)	9(3)		
Si1O7	−2(2)	9(1)		
Si2O2	2(4)	7(4)	9(10)	40(9)
Si2O4	−8(4)	2(3)		
Si2O5	9(2)	17(2)		
Si2O6	5(2)	14(2)		
K Fluor-Richterite				
Si1O1	−1(2)	3(1)	3(1)	33(3)
Si1O5	−4(3)	5(4)		
Si1O6	7.9(2)	15.6(8)		
Si1O7	−2(2)	7(1)		
Si2O2	−7(9)	0(1)	−4(9)	30(9)
Si2O4	−6(2)	5(2)		
Si2O5	9(5)	18(5)		
Si2O6	−1.3(1)	6.8(2)		
andalusite				
SiO2	1(1)	3(1)	5(4)	26(3)
SiO3	1(2)	9(2)		
SiO4	0.2(4)	6.1(5)		
kyanite				
Si1O4	1(5)	5(5)	10(1)	26(1)
Si1O5	5(6)	8(6)		
Si1O8	0(1)	4(1)		
Si1O10	3(1)	8(1)		
Si2O1	5(1)	8(2)	16(5)	29(5)
Si2O3	4(1)	7(2)		
Si2O7	4(2)	7(2)		
Si2O9	1(5)	5(6)		

References

Armbruster, T., Bürgi, H.B., Kunz, M., Gnos, E., Brönnimann, S. and Lienert, C. (1990) Variation of displacement parameters in structure refinements of low albite. American Mineralogist, 75, 135-140.

Boisen, M.B., Jr., Gibbs, G.V., Downs, R.T. and D'Arco, P. (1990) The dependence of the SiO bond length on structural parameters in coesite, the silica polymorphs and the clathrasils. American Mineralogist, 75, 748-754.

Bürgi, H.B. (1989) Interpretation of atomic displacement parameters: Intramolecular translational oscillation and rigid-body motion. Acta Crystallographia, B45, 383-390.

Busing, W.R. and Levy, H.A. (1964) The effect of thermal motion on the estimation of bond lengths from diffraction measurements. Acta Crystallographia, 17, 142-146.

Cameron, M., Sueno, S., Prewitt, C.T. and Papike, J.J. (1973) High-temperature crystal chemistry of Acmite, Diopside, Hedenbergite, Jadeite, Spodumene, and Ureyite. American Mineralogist, 58, 594-618.

Cameron, M., Sueno, S., Papike, J.J. and Prewitt, C.T. (1983) High temperature crystal chemistry of K and Na fluor-richterites. American Mineralogist, 68, 924-943.

Clark, J.R., Appleman, D.E. and Papike (1969) Crystal-chemical characterization of clinopyroxenes based on eight new structure refinements. Mineralogical Society of America Special Paper, 2, 31-50.

Cruickshank, D.W.J. (1956) The analysis of the anisotropic thermal motion of molecules in crystals. Acta Crystallographia, 9, 754-756.

Cruickshank, D.W.J. (1957) A detailed refinement of the crystal structure and molecular structure of naphthalene. Acta Crystallographia, 10, 504-508.

Cruickshank, D.W.J. (1961) Coordinate errors due to rotational oscillations of molecules. Acta Crystallographia, 14, 896-897.

Downs, R.T. (1989) A study of the mean-square displacement amplitudes of T and O atoms in framework silicates and aluminosilicates: Evidence for rigid TO bonds, disorder, twinning and stacking faults in crystals. M.S. thesis, Virginia Polytechnic Institute and State University, Blacksburg, Virginia.

Downs, R.T., Gibbs, G.V. and Boisen, M.B.Jr. (1990) A study of the mean-square displacement amplitudes of Si, Al and O atoms in framework structures: Evidence for rigid bonds, order, twinning, and stacking faults. American Mineralogist, 75, 1253-1267.

Dunitz, J.D., Schomaker, V. and Trueblood, K.N. (1988) Interpretation of atomic displacement parameters from diffraction studies of crystals. The Journal of Physical Chemistry, 92, 856-867.

Harlow, G.E. and Brown, G.E., Jr. (1980) Low albite: an X-ray and neutron diffraction study. American Mineralogist, 65, 986-995.

Hazen, R.M. and Prewitt, C.T. (1977) Effects of temperature and pressure on interatomic distances in oxygen-based minerals. American Mineralogist, 62, 309-315.

Hazen, R.M. and Finger, L.W. (1982) Comparative crystal chemistry. Wiley, New York, New York.

Hirshfeld, F.L. (1976) Can x-ray data distinguish bonding effects from vibrational smearing. Acta Crystallographia, A32, 239-244.

Johnson, C.K. (1969a) An introduction to thermal-motion analysis. In Crystallographic Computing, editor F.R. Ahmed. Munksgaard, Copenhagen.

Johnson, C.K. (1969b) The effect of thermal motion on interatomic distances and angles. In Crystallographic Computing, editor F.R. Ahmed. Munksgaard, Copenhagen.

Levien, L. and Prewitt, C.T. (1981) High-pressure structural study of diopside. American Mineralogist, 66, 315-323.

Megaw, H.D. (1971) Crystal structures and thermal expansion. Materials Research Bulletin, 6, 1007-1018.

Megaw, H.D. (1973) Crystal structures: A working approach. W.B. Saunders Co., Philadelphia, Pa..

Peters, J. and Krebs,B. (1982) Silicon Sisulphide and silicon diselenide: A reinvestigation. Acta Crystallographia, B38, 1270-1272.

Prewitt, C.T. and Young, H.S. (1965) Germanium and silicon disulfides: Structure and synthesis. Science, 149, 535-537.

Schomaker, V. and Trueblood, K.N. (1968) On the rigid-body motion of molecules in crystals. Acta Crystallographia, B24, 63-76.

Smith, J.V., Artioli, G. and Kvick, Å. (1986) Low albite, $NaAlSi_3O_8$: Neutron diffraction study of crystal structure at 13 K. American Mineralogist, 71, 727-733.

Willis, B.T.M. and Pryor, A.W. (1975) Thermal vibrations in crystallography. Cambridge University Press, Cambridge, England.

Winter, J.K., Ghose, S. and Okamura, F.P. (1977) A high-temperature study of the thermal expansion and the anisotropy of the sodium atom in low albite. American Mineralogist, 62, 921-931.

Winter, J.K. and Ghose, S. (1979) Thermal expansion and high-temperature crystal chemistry of the Al_2SiO_5 polymorphs. American Mineralogist, 64, 573-586.

Chapter 2

An Interpretation of the Role of Temperature on the Structural and Dynamic Properties of Quartz

Introduction

Downs et al. (1990) analyzed the mean square displacement amplitudes, MSDAs, for bonded Si and O atoms in a variety of framework silicates and concluded that the SiO bonds in these minerals appear to be rigid (see also Ghose et al. 1986; Bürgi, 1989; Armbruster et al. 1990). Their analysis was based on the 'rigid body hypothesis' (Hirshfeld, 1976) from which they assert that if A and B are atoms in a rigid polyhedron, then the MSDA, z^2_{AB}, of A calculated in the direction of B should tend to equal the MSDA of B calculated in the direction of A, z^2_{BA}, i.e., $z^2_{AB} \approx z^2_{BA}$. They suggest that $\langle\Delta_{SiO}\rangle$, defined as the average $\Delta_{SiO} = z^2_{OSi} - z^2_{SiO}$ for a given silicate tetrahedron, should satisfy the criteria, $-0.00125\text{Å}^2 < \langle\Delta_{SiO}\rangle < 0.002\text{Å}^2$, indicating that the tetrahedron contains rigid SiO bonds. In order to complete the criteria for rigid silicate tetrahedra, the relative motions of the pairs of O atoms must also be considered. If the criteria for rigid SiO bonds is applied to each of the individual bonds, then a corresponding criterion for $\langle\Delta_{OO}\rangle$, the average of $|z^2_{O_iO_j} - z^2_{O_jO_i}|$ for the four oxygens of the silicate group, can reasonably be defined as $\langle\Delta_{OO}\rangle \leq 0.002 - (-0.00125) = 0.00325\text{Å}^2$. If the criteria on $\langle\Delta_{SiO}\rangle$ and $\langle\Delta_{OO}\rangle$ are both satisfied for a given SiO_4 tetrahedron in a framework silicate like quartz, then it may be assumed that the tetrahedron behaves as if it were a rigid body.

Analysis of the Rigid Body Motion of the SiO_4 Tetrahedra in Quartz

Kihara (1990) has undertaken careful structural analyses of quartz over the temperature range between 298 K and 1126 K and has obtained precise anisotropic displacement parameters for the Si and O atoms in both α (low) and β (high)

quartz from which $\langle\Delta_{SiO}\rangle$ and $\langle\Delta_{OO}\rangle$ values were calculated (Table 2–1). In β quartz, the space group symmetry, $P6_222$, assumed in the refinement, constrains the displacement of the O atoms to be equal along all the OO vectors and so their $\langle\Delta_{OO}\rangle$ values must be equal to zero. An examination of Table 2–1 shows that the $\langle\Delta\rangle$ values for both α and β quartz satisfy the criteria stated above, suggesting that the SiO_4 tetrahedra in both of these polymorphs are rigid and that the displacement parameters provide good estimates of the true thermal motion of both Si and O.

The $\langle\Delta_{OO}\rangle$ values for α quartz increase with increasing temperature, with the exception of the one measured at 838 K. An increase of $\langle\Delta_{OO}\rangle$ with increasing temperature has also been observed for other silicates, (Downs et al. 1992) and may indicate a gradual onset of OSiO angle bending modes at elevated temperatures. A calculation of the frequencies for the monosilicic acid molecule, H_4SiO_4, using a 6-31G** basis set, suggests that OSiO modes become active at temperatures in excess of 700 K.

If, as suggested by Buerger (1972) and Boysen et al. (1980), β quartz consists of a disordered array of Dauphiné twinned domains in equal amounts, then the magnitude of the $\langle\Delta_{SiO}\rangle$ values should be comparable ($\sim$ 0.007 Å^2) to those observed for twinned tridymite (Downs et al. 1992). The small $\langle\Delta_{SiO}\rangle$ values recorded in Table 2–1 indicate that β quartz is essentially free of such twins, as suggested by Young (1962) in a careful monitoring of the intensities of selected peaks in the diffraction pattern of quartz as a function of temperature.

If the silicate tetrahedron in quartz behaves as a rigid body, then the motion of its constituent atoms can be separated into translational, librational and screw–correlated components of motion by undertaking a TLS analysis of the displacement parameters of the five atoms in the group, using the strategies described

Table 2–1. Rigid body parameters for SiO bond stretching, $\langle\Delta_{SiO}\rangle$, and for OSiO angle bending, $\langle\Delta_{OO}\rangle$, the displacement of the O atom from the β position, $D_{\alpha\beta}$, and the root–mean square displacement amplitude due to libration, $z_{\alpha\beta}$, calculated at a variety of temperatures, using Kihara's data (1990). The errors on $D_{\alpha\beta}$ and $z_{\alpha\beta}$ are estimated to be 0.002Å.

T (K)	$\langle\Delta_{SiO}\rangle$ (Å^2)	$\langle\Delta_{OO}\rangle$ (Å^2)	$D_{\alpha\beta}$ (Å)	$z_{\alpha\beta}$ (Å)
		α quartz		
298	0.00038	0.00062	0.394	0.083
398	0.00059	0.00065	0.381	0.099
498	0.00034	0.00087	0.365	0.109
597	0.00056	0.00092	0.345	0.128
697	0.00051	0.00132	0.315	0.148
773	0.00045	0.00148	0.282	0.165
813	0.00091	0.00174	0.254	0.180
838	0.00110	0.00145	0.204	0.204
		β quartz		
848	0.00021	0.00000	0.000	0.272
854	0.00091	0.00000	0.000	0.269
859	0.00069	0.00000	0.000	0.267
869	0.00068	0.00000	0.000	0.269
891	0.00079	0.00000	0.000	0.267
920	0.00115	0.00000	0.000	0.265
972	0.00073	0.00000	0.000	0.265
1012	0.00167	0.00000	0.000	0.265
1078	0.00069	0.00000	0.000	0.266

by Schomaker and Trueblood (1968). The results of such an analysis imply that the motion of the Si atom in quartz is almost entirely translational, with little or no librational component. If true, then the thermal motion of the O atoms must embody all of the motion of the Si atom plus that ascribed to the libration of the SiO_4 group. Downs et al. (1992) have also obtained results that seem to imply that the motion of the Si atom in a variety of high temperature silicate structures is almost entirely translational.

Translational motion in a crystal manifests itself as low frequency, long wavelength acoustical waves. As such a motion is characterized by a large number of unit cells being displaced in tandem, this motion cannot be considered as a major factor in the $\alpha \rightleftharpoons \beta$ transition when examined at the level of the unit cell. Consequently, the behavior of quartz with temperature should correlate with the librational component of motion. Therefore, the displacement amplitudes of the O atoms, ascribed to the librational component of motion of the silicate group, may be used to characterize the transition.

A Configurational Potential for the $\alpha \rightleftharpoons \beta$ Transition

The heat content of quartz, as determined by Mosesman and Pitzer (1941), was found by Young (1962) to correlate with the vibrational amplitude, and thus the vibrational energy, of the bridging oxygen. Accordingly, the variation in the shape and the magnitude of the ellipsoid of the oxygen atom should also reflect the character of the potential energy in the vicinity of the atom. An analysis of the thermal displacements of the oxygen atom as a function of temperature was undertaken to test this assertion, using Kihara's (1990) data. This analysis yields a configurational potential for quartz.

In this analysis, the librational contribution to the rms displacement amplitude of the O atom, denoted $z_{\alpha\beta}$, was calculated in the direction of the vector connecting the position of the O atom in α quartz to that in β quartz. This vector is defined to radiate from the α_1 position in the direction of the α_2 position such that its magnitude, $D_{\alpha\beta}$, is one half the distance between the two. A comparison of the resulting $z_{\alpha\beta}$ values with $D_{\alpha\beta}$ is given in Table 2–1 for the data recorded between 298 K and 1078 K by Kihara (1990). In particular, just as the phase transition is about to occur, at 838 K, $D_{\alpha\beta}$ is observed to equal $z_{\alpha\beta}$. This supports both Young's (1962) and Megaw's (1973) assertion that the transition occurs when $z_{\alpha\beta}$

equals $D_{\alpha\beta}$.

The data in Table 2–1 was used to construct a configurational potential energy diagram for the $\alpha \rightleftharpoons \beta$ quartz transition (Figure 2–1). In this diagram, both the α_1 (left–handed quartz) and α_2 (right–handed quartz) displacements are plotted, assuming that their values are equal but opposite in sign, consistent with the space group symmetries of left– and right–handed quartz. The vertical centerline in the figure locates the position of the O atom in β quartz, and the points plotted as plus signs, (+), locate the mean displacements of the O atom in α quartz from their position in β quartz, $D_{\alpha\beta}$, at the given temperatures. Asterisks, (*), plotted on either side of the plus signs, define the librational rms displacement amplitudes of the O atoms, $z_{\alpha\beta}$. These points are joined to form the configurational potential energy curve displayed in the figure. At a given temperature, the O atoms are considered to be oscillating back and forth between the sides of the curve with their mean positions located at the plus signs. The figure shows a potential well with a double minimum for α quartz and a potential well with a single minimum for β quartz superimposed above.

The outer limits of the double well are more or less vertical until about 700 K where they curve inward. This change in the curve can be ascribed to either the effects of incipient tunneling from one α domain to the other or to the effect of a thermal distribution of vibrational states in which some of the energies are above the $\alpha \rightleftharpoons \beta$ transition energy. There seems to be no apparent way to distinguish between these effects using the atomic displacement parameters. Nevertheless, it is clear that the magnitudes of the displacement parameters are influenced by more than the thermal motion starting at temperatures about 150° below the $\alpha \rightleftharpoons \beta$ transformation temperature, T_C. The single well for the β phase curves slightly inwards for the first 75° above T_C, consistent with observations by Kihara

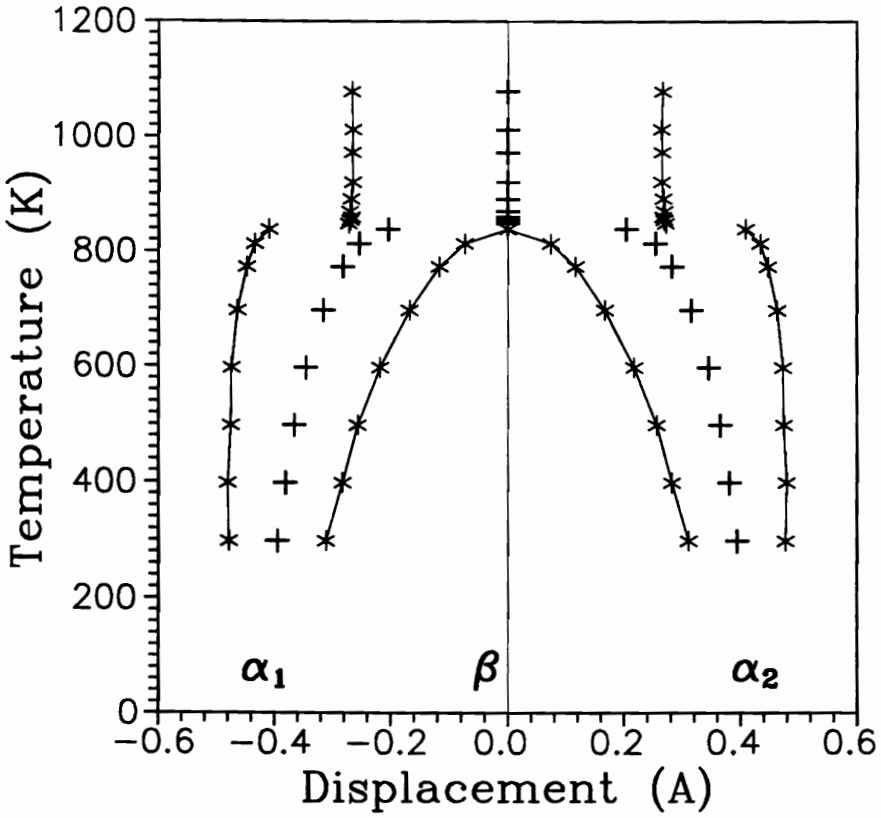

Figure 2–1. A configurational potential energy diagram constructed from the librational displacements of the rigid body motion of the silicate tetrahedra in quartz with temperature. The curve shows a double well for α quartz and a single well for β quartz. See the text for a full discussion.

(1990) that the temperature factor of the oxygen atom decreases in magnitude over the same temperature interval. If a thermal distribution of vibrational states is assumed in which some energies are below T_C, then the displacement parameters should be elongated toward the atoms still in α positions. However, using Equation 1–2 , the values in Table 2–1 indicate that only ~0.2% of the crystal would still be in the α phase at 848 K.

The Interatomic Forces

The vertical nature of the outer portions of the double well suggests the presence of interatomic forces that limit the oscillatory motion of the SiO_4 group in

the direction away from the β position. Therefore, as the temperature of the crystal is increased and the amplitude of oscillation of the SiO_4 group increases, the O atom is indicated to vibrate more toward the β position than away from it. This implies that the mean position of the O atom moves progressively toward the β position and that the value of $D_{\alpha\beta}$ decreases with increasing temperature. The double well for quartz is traditionally pictured as the superposition of two harmonic wells. This picture is inconsistent with Figure 2–1 in that the outer portions of the well are much too steep for a pure harmonic model.

To improve the understanding of the $\alpha \rightleftharpoons \beta$ transformation in terms of structural changes in quartz, it would be useful to know the extent to which the forces that govern the SiO bond length and the SiOSi and OSiO angle variations are responsible for the shape of the double well. Assuming that the structure consists of rigid SiO_4 tetrahedra, Megaw (1973) has argued, on the basis of the work by Young (1962), that the barrier in this well results from an increase in energy that accompanies the relatively large change in the SiOSi angle from 144° at room temperature to 153° at the transformation temperature. A potential energy curve calculated in this study as a function of the SiOSi angle supports her arguments.

Using the SQLOO potential energy function developed by Boisen and Gibbs (submitted) to describe the pressure behavior of α quartz, cristobalite and coesite, a calculation was undertaken with the software MADMAX, to model the configurational potential displayed in the figure. The SQLOO energy function, used in the calculation, employs regressor values set to the SiO bond lengths and the OSiO and SiOSi angles that were calculated for the molecule $H_6Si_2O_7$, using a robust 6-31G* basis set. In addition, each of the regressor values was weighted with force constant data calculated for the molecule. Since compression is not involved in this study, the nonbonded OO repulsion term in the SQLOO model,

designed to maintain reasonable non–codimer OO separations at high pressures, was found to make a negligible contribution to the results and hence its effects will be ignored.

In the calculations, even though only $P1$ symmetry was assumed for the model, the atoms arranged themselves with the $P3_221$ symmetry observed for α quartz when the structural parameters were allowed to vary until a minimum energy was calculated. In a subsequent series of calculations, the unit cell volume was systematically constrained to larger and larger volumes. For each volume, the structural parameters were varied, subject to $P3_221$ symmetry, until they arrived at a lowest energy configuration. At some volume all of the positional parameters simultaneously adopted the higher $P6_222$ symmetry arrangement. This volume is assumed to correspond to the energy at which the phase transition occurs.

In an analysis of those calculations associated with the α phase, the cell dimensions and the positional parameters of the atoms were found to vary in a uniform way except that for the x–coordinate of the O atom which shows a small but distinct discontinuity at an estimated temperature of 800 K. An examination of the structures generated on both sides of this discontinuity shows that they are identical except for the switching of the long and short SiO bonds. Kihara's (1990) data shows the same phenomenon with SiO(1) increasing from 1.596Å to 1.600Å and with SiO(2) decreasing from 1.604Å to 1.594Å as the temperature increases from 773 K to 813 K. The 800 K estimate of the temperature for the modeled discontinuity was made by matching the calculated value for $D_{\alpha\beta}$ with that observed for quartz (Kihara, 1990) at a given temperature. It may be pertinent that the high temperature data recorded for cristobalite by Peacor (1973) show a similar result with the two nonequivalent SiO bonds switching in length at a temperature near 450 K.

Three additional SQLOO calculations were made to ascertain the structural changes that are responsible for the shape of the double well. In the first, the force constants of all of the regressor values were set equal to zero except that for the SiOSi angle, in the second, all of the force constants were set equal to zero except those for the individual SiO bonds and their cross terms, and in the third, all force constants were set equal to zero except for those of the OSiO angles. The displacements of the O atom from the β position was calculated for each of the minimum energy configurations and are plotted against the energies obtained in these four calculations in Figure 2–2a.

The curve calculated with the full SQLOO model shows a double well that conforms very nicely with that displayed in Figure 2–1, except for the failure to reproduce the same degree of steepness in the outer portions. This is not too surprising in that the SQLOO model is almost entirely harmonic (Boisen and Gibbs, submitted). The curve calculated with only the SiOSi contribution to the energy matches that calculated with the full model except that the barrier is lower and the sides of the well are less steep. The curve calculated with only the SiO contribution shows a much smaller barrier. The barrier is absent in the calculation when only the OSiO angles are considered. These results indicate that the forces associated with the bridging angle play a dominant role ($\sim$75%) in governing the $\alpha \rightleftharpoons \beta$ phase transformation of quartz while those for the SiO bonds play a minor role ($\sim$15%). Just below T_C, the calculations indicate that the bridging O atom is librating about its equilibrium position with a concomitant change in the SiOSi angle of $\pm 10°$. This is more than twice the value, $\pm 4°$, calculated for the room temperature structure. As the temperature is raised, extra thermal energy is required to promote the increase in oscillation of the bridging O. Therefore, the specific heat should increase sharply as the temperature approaches T_C, providing

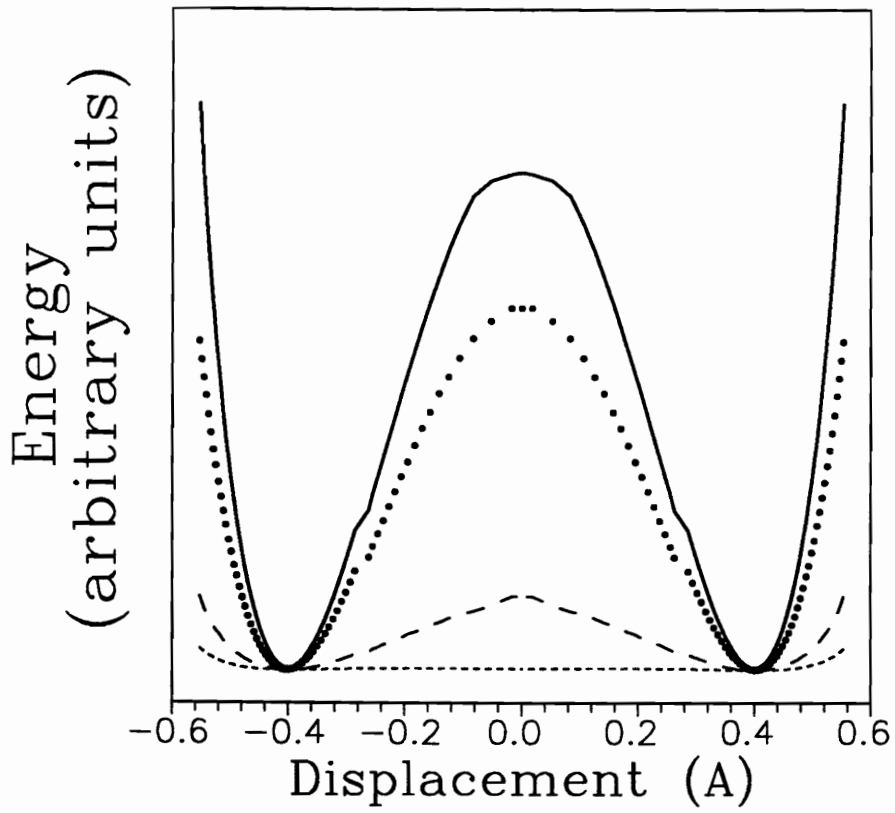

Figure 2–2a. The calculated potential double well for α quartz is outlined with the solid line while the dotted curve is the contribution to the total energy from SiOSi angle bending, the long dashed curve is the contribution from SiO bond stretching and the short dashed curve is from OSiO angle bending forces. The SiOSi angle bending forces contribute the greatest amount (75%) to the total energy of this potential.

an explanation for the lambda point observed in the heat capacity curve for quartz (Mosesman and Pitzer, 1941).

A SQLOO model of the potential well for β quartz was generated in a series of calculations in which the position of the O atom was moved along the $\alpha - \beta$ vector, using the cell dimensions observed at 848 K by Kihara (1990). Three additional calculations were completed in which all of the force constants were set equal to zero except that for the SiO bond, the SiOSi angle and the OSiO angle, as described above. The results of these calculations are plotted in Figure 2–2b

as a function of the displacement of the O atom from its β position. Unlike the data plotted in Figure 2–2a, a single well is generated in the full calculation. The plots generated with all of the force constants set to zero except for SiO and for OSiO show that the potentials for these parameters parallel that obtained in the full calculation. On the other hand, that generated for the SiOSi curve shows a maximum at the β–position, as found for α quartz. This causes the bottom of the well, calculated with all of the parameters included, to be flattened. Such a result was anticipated by Young (1962) who predicted, assuming anharmonic coupling of vibrational modes, a single well for β quartz with a somewhat flattened bottom. Such a coupling has since been confirmed by Scott (1968) in a study of the temperature dependent Raman spectrum of quartz and by Boysen et al. (1980) from inelastic neutron scattering studies of interacting modes.

An important question raised by Young (1962) is whether the double minimum potential well for the α phase persists into the stability field of the β phase or whether it is replaced by a single minimum well. Insight into this question is provided by the model, by an analysis of Kihara's (1990) data and by the Yamamoto et al. (1988) observation that sharp triangular microdomains of Dauphiné twins disappear at temperatures above T_C.

The experimental data in Figure 2–1 and the model data in Figure 2–2 both show a double well dominated by SiOSi interactions for the α phase and a single well dominated by SiO interactions for the β phase. Based on these figures the temperature induced behavior of quartz will be interpreted. Since the double well does not persist into the stability field of β quartz, it is concluded that the $\alpha \rightleftharpoons \beta$ transformation is not a second order transition but rather a first order one. In addition, the inward curving of the outer limits of the double well indicates that there is another type of transition taking place at temperatures below T_C that

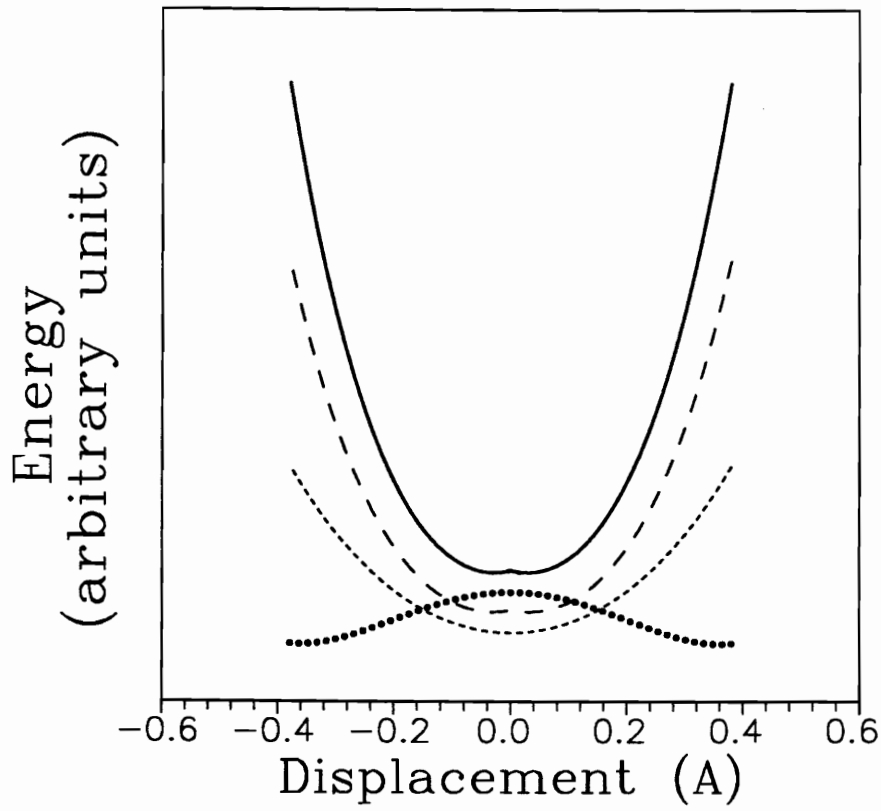

Figure 2–2b. A plot of the modeled configurational potential energy curve for β quartz. The total energy is represented by the solid curve, the SiO bond stretching contribution to the energy is represented by the long dashed curve, the OSiO angle bending contribution is represented by the short dashed curve and the SiOSi bending contribution is represented by the dotted curve. In contrast with Figure 2–2a, it is apparent that forces associated with the stretching of the SiO bonds make the greatest contribution to the total energy of this potential.

involves the transformation of α quartz into its enantiomorph, i.e., $\alpha_1 \rightleftharpoons \alpha_2$. This transformation appears to be a second order transition that involves positional disorder of the oxygen atom about the [210] zone of the structure.

As the temperature is raised, the amplitude of oscillation of the O atom increases (Figures 2–1 and 2–2). Associated with this increased amplitude, there is an increased flexing of the SiOSi angle, the angle decreasing as the libration of the tetrahedron takes the O atom away from the β position and increasing as the

O atom is taken toward the β position. It is important, however, to keep in mind that the potential energy curve for the SiOSi angle is asymmetric, as illustrated by a series of MP2 calculations on the molecule $H_6Si_2O_7$ completed with a robust 6–31G** basis set (Figure 2–3). Consequently, when the O atom oscillates in the direction away from the β position, the potential energy increases rapidly. On the other hand, when it oscillates toward the β position, the potential energy still increases, but less rapidly. Thus, the mean position of the O atom is expected, as observed, to gradually move toward the β position as the amplitude of oscillation increases, with a concommitant increase in the SiOSi angle and decrease in the tilt angle of the silicate group. As the mean position of the O atom moves toward the β position, both the width and the height of the barrier decrease (Figures 2–1 and 2–2). This implies that both tunneling and positional disorder should take place among the α_1 and α_2 phases, consistent with the second order phase transition. Furthermore, as the temperature of the crystal is raised, the separation in energy between vibrational modes for the α and the β phases decreases with a concomitant conversion of small parts of the crystal into the β phase. It is suggested that at temperatures approaching the top of the barrier (Figures 2–1 and 2–2), just below T_C, the second order transformation is completed and there are equal amounts of triangular microdomains of α_1 and α_2 quartz. It also appears on the basis of the dark field images recorded for quartz near T_C (Yamamoto et al. 1988), that these domains form an ordered periodic pattern of alternating α_1 and α_2 triangles which are in perpetual migration. The existence of this array of migrating microdomains, referred to as the incommensurate phase, was first observed by Van Tendeloo et al. (1976) in their study of the triangular Dauphiné twin domains exhibited by quartz. At T_C, Figure 2–1 indicates that the mean position of the O atom is suddenly displaced to the β position. Above this temperature,

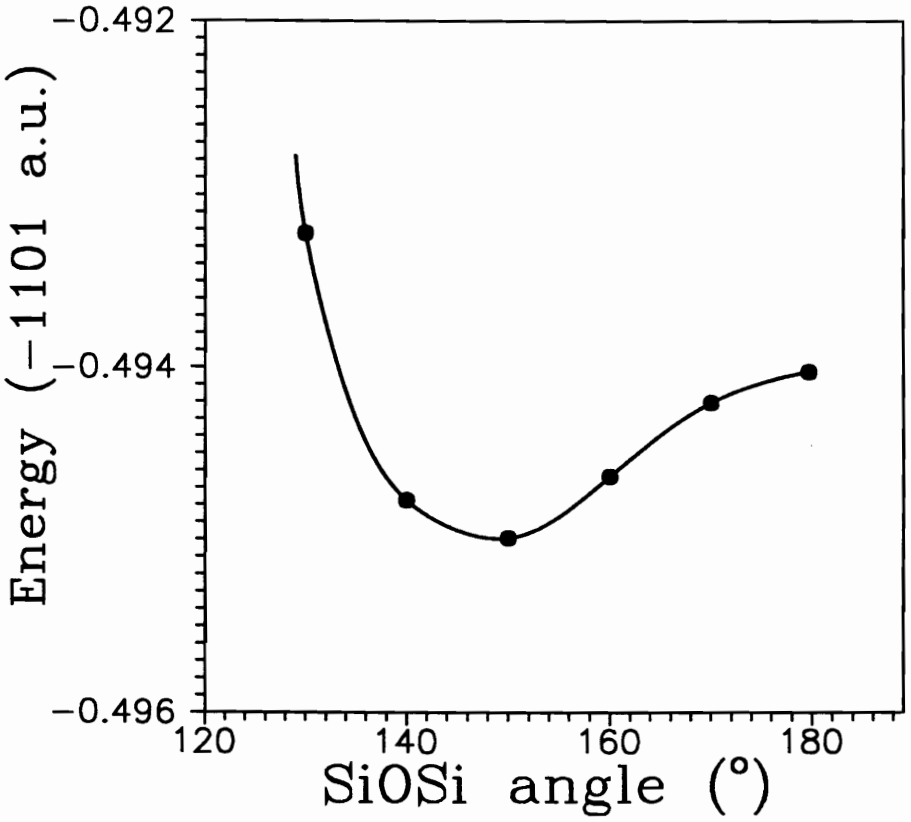

Figure 2–3. This figure shows a plot of the anharmonic potential energy curve calculated as a function of the SiOSi angle for the molecule $H_6Si_2O_7$. In the calculation, the molecular geometry was first optimized assuming C_{2v} point symmetry with the OSiO angles fixed at $\cos(-1/3)$, using a MP2 6-31G** basis set. The optimized parameters are: $R(SiO_{br}) = 1.609$Å, $R(SiO_{nbr}) = 1.638$Å, $\angle$ SiOSi = 147.43°. The SiOSi angle was then clamped at the values given in the figure and the SiO_{br} was optimized yielding the following bond lengths for each of the angles: 180°, 1.595Å; 170°, 1.596Å; 160°, 1.601Å; 150°, 1.607Å; 140°, 1.614Å; 130°, 1.624Å; 120°, 1.638Å; 110°, 1.664Å.

the O atom vibrates in a symmetric but anharmonic well with the β phase replacing the triangular microdomains associated with the incommensurate phase. It is noteworthy that at temperatures above T_C, the mean SiOSi angle remains essentially constant, a fact that can be explained by the symmetrical nature of the well displayed in Figure 2–2b.

Configurational Equi–Potential Energy Contours Around the Oxygen Atom

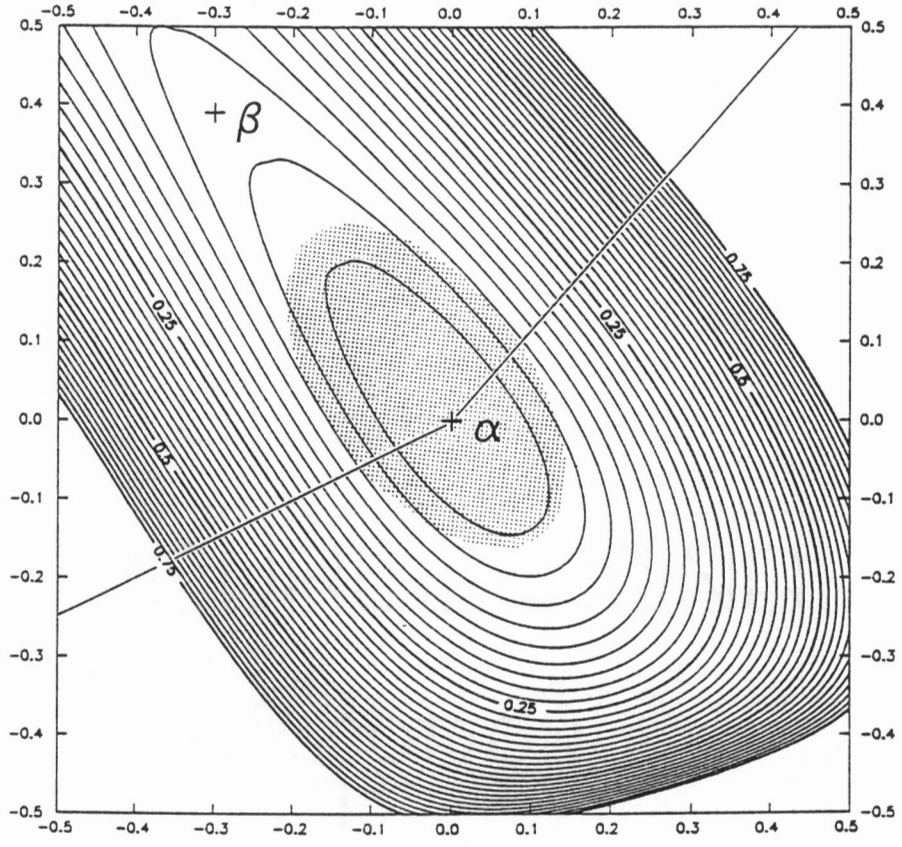

Figure 2–4a. A 1Å^2 energy contour diagram in the $y-z$ plane, centered about the modelled position of the O atom in the α phase. The energy is in atomic units. The two plus signs indicate the positions of the atom in the α and the β phases. The two SiO bond vectors are projected onto the plane to demonstrate the influence of the SiO bond stretching forces on the orientation of the well. For comparison, the observed thermal displacement ellipsoid of the O atom at 597 K is also projected onto the plane as the stipled region. Note that its center is displaced toward the β position and that it is oriented in a manner conforming with the energy contours.

The configurational energy in the vicinity of the O atom in quartz was calculated with the SQLOO energy function to gain insight into the potential about the atom (Figure 2–4), assuming a fixed position for the Si atom. A calculation

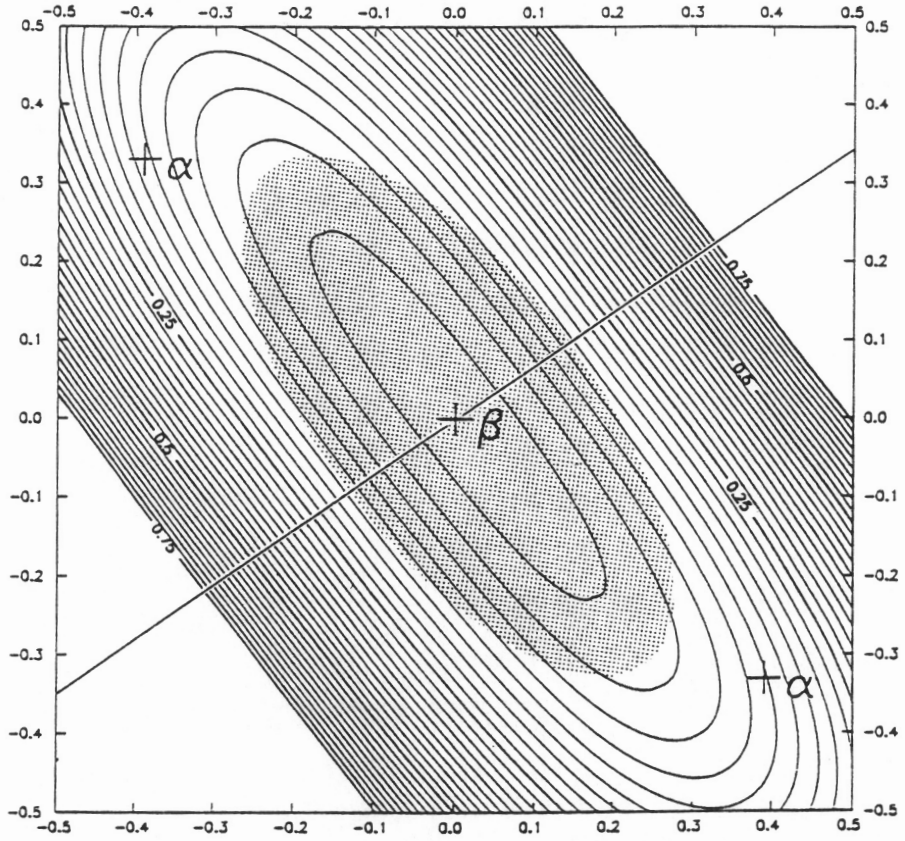

Figure 2–4b. A 1Å^2 energy contour diagram in the $y-z$ plane, centered about the position of the O atom in the β phase. The observed thermal ellipsoid of the O atom at 891 K is projected onto the plane. Note that the center of the thermal ellipsoid and the energy contours is fixed and does not vary with temperature in the β phase.

was completed for the plane

$$P = \{0.4133, y, z | 0.1653 \leq y \leq 0.3687, 0.0265 \leq z \leq 0.2115\}$$

which defines a 1Å $\times$ 1Å plot containing the $\alpha - \beta$ path for α quartz (Figure 2–4a). A similar 1Å $\times$ 1Å plot for β quartz is presented in Figure 2–4b. The plus signs in both figures define model determined positions for the O atom in the α and β phases. Figure 2–4a shows an asymmetric well, with its minimum at the α position, elongated toward the β position. An examination of the model indicates

that the direction of the elongation of the well is governed almost entirely by the SiO stretching force constant as illustrated by the projection of the two SiO bond vectors onto the plane. The shape of this well provides an explanation for the observed displacements of the O atom in α quartz as a function of temperature. Assuming that the O atom oscillates within the confines of an energy contour, then the mean position of the atom will be at the geometric mean of that contour. The close correspondence that obtains between the orientation of the displacement ellipsoid observed for quartz at 597 K and the energy contours is also depicted in the figure. With increasing oscillation, the mean position of the O atom will be progressively and linearly displaced in the direction of the β position. This displacement continues until T_C where it adopts the position observed in β quartz.

The contours in the map calculated for β quartz, unlike those calculated for α quartz, are centered about the β position. This provides an explanation of why the position of the O atom is independent of temperature in β quartz. Again, as displayed in Figure 2–4b, the orientation of the observed displacement ellipsoid conforms very nicely with the energy contours. However, the orientation of the ellipsoid does not parallel the $\alpha - \beta$ line as it does for α quartz. Young (1962) was the first to observe this change in orientation. However, he considered this change to be an artifact of the refinement model rather than a natural result of the energetics of the system.

The role of π bonding as a driving mechanism for the $\alpha \rightleftharpoons \beta$ transition

In 1961, Cruickshank asserted that the $3d_{z^2}$ and $3d_{x^2-y^2}$ orbitals on the Si atom in a SiO_4 group overlap with selected p–orbitals on the O atoms, forming a $(d-p)\pi$ bond, in which the order of the bond was indicated to increase with increasing SiOSi angle. Grimm and Dorner (1975) observed that the SiO bond lengths for quartz recorded by Young (1962) over a wide range of temperatures,

vary inversely with angle, in conformity with Cruickshank's assertion that shorter SiO bonds should involve wider SiOSi angles. This led them to suggest that the π bond order was the driving mechanism for the $\alpha \rightleftharpoons \beta$ transition of quartz, with the order of the bonds increasing with temperature. Thus, with increasing temperature, not only would the SiO bond lengths in the mineral be expected to decrease, but the SiOSi angle would also be expected to widen. An examination of the apparent SiO bond lengths recorded as a function of temperature (Figure 2–5) shows that while they decrease significantly with increasing temperature in α quartz, they are independent of temperature in β quartz (Kihara, 1990). Further examination also shows that the SiOSi angle widens about 10° when quartz is heated from room temperature to T_C.

It is important to note that the SiO bond lengths used to prepare the lower plot in Figure 2–5 were not corrected for thermal motion, and therefore represent apparent interatomic separations rather than mean interatomic separations. Grimm and Dorner (1975) based their conclusion on such a plot. However, since the silicate tetrahedra in quartz seem to behave as rigid groups, the mean interatomic bond lengths can be estimated by correcting Kihara's bond length data for thermal motion effects, using the simple rigid bond model derived by Downs et al. (1992). The corrected bond lengths, plotted as a function of temperature (upper part of Figure 2–5), increase, rather than decrease, in a regular way in both α and β quartz, with the rate of increase in β quartz being three times as great as that in α quartz. The greater expansion rate of the bond in β quartz is expected in view of Figure 2–2 where it is seen that the variation of the energy associated with a given change in the SiO bond length in α quartz is small relative to that in β quartz. As it is the mean interatomic separations that have chemical significance, the assertion that the π bond order is the driving mechanism for

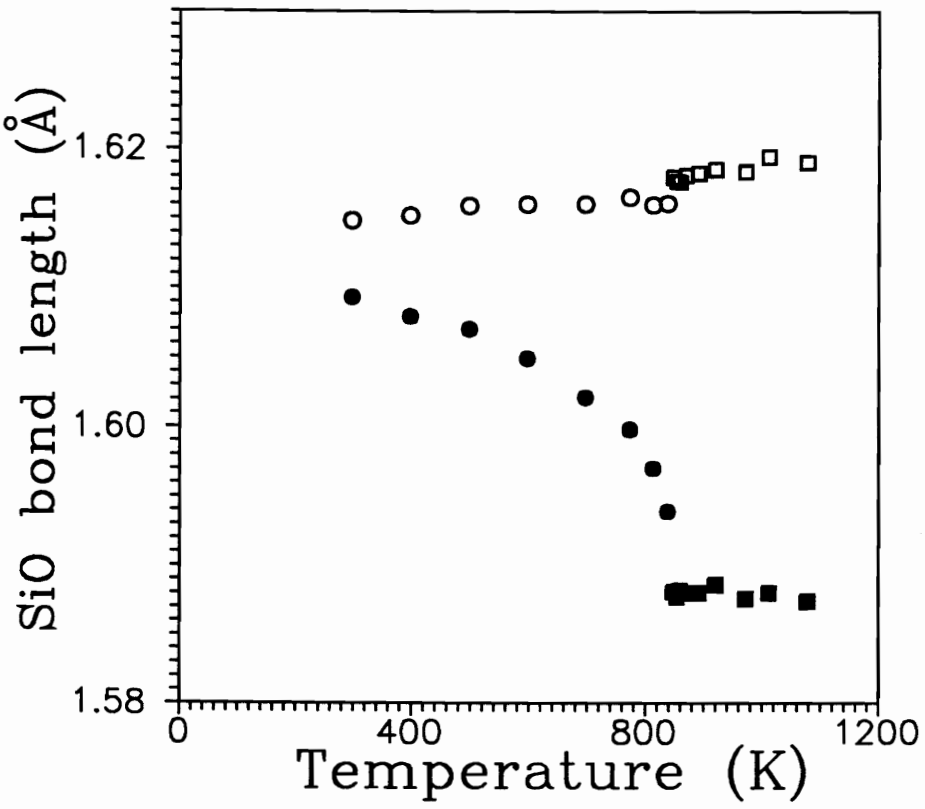

Figure 2–5. The variation of the apparent and the thermally corrected SiO bond lengths as functions of temperature in quartz. The apparent observed bond lengths (Kihara, 1990), are plotted as solid circles for α quartz and solid squares for β quartz. The mean SiO bond lengths, corrected for thermal motion, are plotted as open circles for α quartz and as open squares for β quartz. The two non–equivalent bond lengths in α quartz are averaged. The apparent bond lengths decrease dramatically in α quartz as temperature increases, but remain relatively constant in β quartz. On the other hand those corrected for thermal motion increase systematically with temperature. The corrected bonds in α quartz are found to vary as $R_m = 1.6144(4) + 2.3(6) \times 10^{-6}T$ while in β quartz they vary as $R_m = 1.612(1) + 7(1) \times 10^{-6}T$.

the phase transition in quartz is not substantiated because the SiO bond length is seen to increase rather than decrease as the SiOSi angle and the temperature increase.

References

Armbruster, T., Bürgi, H.B., Kunz, M., Gnos, E., Brönnimann, S. and Lienert, C. (1990) Variation of displacement parameters in structure refinements of low albite. American Mineralogist, 75, 135-140.

Boysen, H., Dorner, B., Frey, F. and Grimm, H. (1980) Dynamic structure determination for two interacting modes at the M–point in α– and β–quartz by inelastic neutron scattering. The Journal of Physics C: Solid State Physics, 13, 6127-6146.

Buerger, M.J. (1972) Phase transformations. Soviet Physics–Crystallography, 16, 959-968.

Bürgi, H.B. (1989) Interpretation of atomic displacement parameters: Intramolecular translational oscillation and rigid-body motion. Acta Crystallographia, B45, 383-390.

Cruickshank, D.W.J. (1961) The role of *3d*-orbitals in π-bonds between (a) silicon, phosphorus, sulfur, or chlorine and (b) oxygen or nitrogen. The Journal of the Chemical Society, 1077, 5486-5504.

Downs, R.T., Gibbs, G.V. and Boisen, M.B.Jr. (1990) A study of the mean-square displacement amplitudes of Si, Al and O atoms in framework structures: Evidence for rigid bonds, order, twinning, and stacking faults. American Mineralogist, 75, 1253-1267.

Downs, R.T., Gibbs, G.V., Bartelmehs, K.L. and Boisen, M.B.Jr. (1992) Variations of bond lengths and volumes of silicate tetrahedra with temperature. American Mineralogist, 77, 751-757.

Ghose, S., Schomaker, V. and McMullan, R.K. (1986) Enstatite, $Mg_2Si_2O_6$: A neutron diffraction refinement of the crystal structure and a rigid-body analysis of the thermal vibration. Zeitschrift für Kristallographie, 176, 159-175.

Grimm, H. and Dorner, B. (1975) On the mechanism of the $\alpha - \beta$ phase transformation of quartz. The Journal of the Physical Chemistry of Solids, 36, 407-413.

Hirshfeld, F.L. (1976) Can x-ray data distinguish bonding effects from vibrational smearing?. Acta Crystallographia, A32, 239-244.

Kihara, K. (1990) An X-ray study of the temperature dependence of the quartz structure. European Journal of Mineralogy, 2, 63-77.

Megaw, H.D. (1973) Crystal structures: A working approach. W.B. Saunders Co., Philadelphia, Pa.

Mosesman, M.A. and Pitzer, K.S. (1941) Thermodynamic properties of the crystalline forms of silica. Journal of the American Chemical Society, 63, 2348-2356.

Schomaker, V. and Trueblood, K.N. (1968) On the rigid-body motion of molecules

in crystals. Acta Crystallographia, B24, 63-76.

Scott, J.F. (1968) Evidence of coupling between one– and two–phonon excitations in quartz. Physical Review Letters, 21, 907-910.

Van Tendeloo, G., Van Landuyt, J. and Amelinckx, S. (1976) The $\alpha \rightarrow \beta$ phase transition in quartz and $AlPO_4$ as studied by electron microscopy and diffraction. Physica Status Solidi, 33A, 723-735.

Yamamoto, N., Tsuda, K. and Yagi, K. (1988) High voltage electron microscope study of incommensurate phase in quartz. Journal of the Physical Society of Japan, 57, 1352-1364.

Young, R.A. (1962) Mechanism of the phase transition in quartz. Air Force Office of Scientific Research, Report 2569, Washington 25, D.C..

Chapter 3

The Pressure Behavior of α–Cristobalite

Introduction

β–cristobalite is the cubic phase of the SiO_2 silica polymorphs that is stable at room pressure and at temperatures between 1743 K and the melting point near 1900 K. The structure exists in a metastable state at temperatures between ~500 K and 1743 K. Near 500 K it undergoes a 'first order reversible phase transformation' to a tetragonal form, α–cristobalite, which is also metastable. The temperature behavior of α and β cristobalite has been studied extensively and is reviewed by Hatch and Ghose (1991).

Recently, there has been interest in developing mathematical models that can describe and predict the structural behavior of the silica polymorphs at pressures (Sanders et al. 1984; Lasaga and Gibbs, 1987, 1988; Gibbs et al. 1988; Stixrude and Bukowinski, 1988; Tsuneyuki et al. 1988; Cheilikowsky et al. 1990; van Beest et al. 1990; Boisen and Gibbs, submitted). It is important to have experimentally determined volume and structural data collected at pressure for a comparison and testing of these models. Such data are available for quartz, coesite and stishovite. Only volume compressibility has been determined for cristobalite (Tsuchida and Yagi, 1990; Yeganeh–Haeri et al. 1990; 1992), but no structural determinations have been reported as a function of pressure. In this paper, volume and structural data are reported at pressures up to 1.6 GPa for single crystal cristobalite, providing a data set that can be used to test a theoretical model.

Room Temperature Single Crystal Structure Refinement

The cristobalite crystals used in this study, collected from Ellora Caves, Hyderabad State in India (Van Valkenburg and Buie, 1945), were kindly supplied by Carl Francis of the Harvard University Museum (Specimen No. 97849). They

occur as single and spinel twinned gem quality octahedra in vesicles of Deccan basalt, perched on fibers of mordenite in association with paramorphs of quartz after cristobalite. Untwinned crystals were found and distinguished from the quartz paramorphs by the differences in their refractive indices. In a study of the $\alpha - \beta$ inversion of cristobalite, Peacor (1973) concluded that these crystals probably formed at temperatures below ~500 K.

A single fragment from a crushed octahedron, with approximate dimensions 125 x 100 x 40 μm, was chosen for a single crystal X-ray diffraction study at room temperature and pressure. A number of peaks in the diffraction pattern were scanned to ensure that they were well–formed and that no peaks ascribable to twinning were present. The crystal was found to have space group symmetry $P4_12_12$ with cell dimensions a=4.9717(4)Å and c=6.9223(3)Å (Table 3–1). A complete sphere of intensity data, I_{hkl}, was collected to $\sin\theta/\lambda = 0.7\text{Å}^{-1}$ on a Rigaku AFC–5 diffractometer with monochromated MoK_α radiation ($\lambda = 0.7093$ Å) generated from a rotating anode. A total of 1958 I_{hkl}–data were collected and corrected for type I isotropic extinction (Becker and Coppens, 1975). No absorption correction was applied because the linear absorption coefficient was small (μ_L=8.545 cm^{-1}). An averaging of the symmetry equivalent reflections resulted in a disagreement index on $|F|$ of 0.018. Of the 171 nonequivalent observations, 146 had $I_{hkl} \geq 2\sigma_F$. The structure was refined with anisotropic temperature factors to a weighted residual of 1.0%, using a revised version of RFINE6 (Finger and Prince, 1975). The refined structural parameters and the conditions of refinement are given in Table 3–2. A comparison of the observed and calculated diffraction data is given in the Appendix. Additional refinements were undertaken with one and with two twin components, according to the twin laws suggested by Dollase (1965). Twin components, if present at all, appear to be less than 1%.

The structure of cristobalite consists of a framework of corner–sharing SiO_4 silicate tetrahedra, each with two non–equivalent SiO bond lengths of 1.603Å, linked together with SiOSi angles of 146.49°. Despite equal bond lengths, the SiO_4 tetrahedra are more distorted than those in either quartz or coesite, two other well–ordered structure types of silica. The OSiO angles of the tetrahedra vary between 108.2° and 111.4°, with a tetrahedral angle variance of 1.56°. The tetrahedral angle variances for quartz and coesite are smaller, ranging between 0.2° and 0.8°. Since all SiO bonds are equal in length, it is not apparent why the OSiO angles depart from $\cos(-1/3)$, given the correlations found between $f_S(T)$ and bond length (Boisen and Gibbs, 1987; Boisen et al. 1990). Selected interatomic angles and bond lengths (Table 3–3) are in reasonable agreement with the values reported by Dollase (1965), Peacor (1973) and Pluth et al. (1985).

The thermal parameters for Si and O are large compared with those obtained for quartz or coesite. This was a matter of concern because large temperature factors are often a sensitive indicator of a twinned or disordered structure. For example, an analysis of the magnitude of the large thermal displacements of the O atom in high cristobalite led Nieuwenkamp (1937) to deduce its dynamically disordered state. In a more recent study, Dollase (1965) concluded that the large thermal parameters in low cristobalite were an artifact of the refinement, resulting from correlations with the scale factor. However, since the correlation between B(O) and B(Si) was observed to be smaller, he concluded that the ratio of the thermal parameters was more meaningful than their individual magnitudes. On the other hand, Peacor (1973) did not observe this high correlation, but he did observe that the orientation of the thermal ellipsoids in cristobalite is consistent with a mechanical model of oscillatory motion in which the major axis of the O atom is oriented approximately normal to the SiOSi plane, a direction which

minimizes SiO bond stretching.

In this study, the largest correlation found (0.46) was between the scale factor and β_{11} for the Si atom. As the remaining correlations are significantly smaller than 0.46, the problem of correlation is concluded as insignificant. An examination of the orientations of the thermal ellipsoids shows that the major axis of the O atom is oriented normal to the SiOSi plane to within 5°. Moreover, the differences in the displacement parameters of the Si and O atoms indicate that the SiO_4 tetrahedra behave as rigid bodies, a conclusion that obtains when the displacement parameters represent thermal motion only, with no component of static disorder (Downs et al. 1990). In summary, the large displacement parameters recorded for the Si and O atoms in cristobalite can simply be ascribed to large amplitudes of vibration.

The thermal ellipsoids in well–ordered structures can be considered as representing time averaged quadratic surfaces of equal configurational potential energy about the mean position of an atom. A careful analysis of the size, shape and orientation of the ellipsoid of the O atom in quartz has, for example, provided insight into the nature of its potential well (Chapter 2). As observed above, earlier studies have shown that the thermal motion of the Si and O atoms in framework silicates is consistent with the motion of rigid tetrahedra. Very small amplitudes of oscillation are associated with SiO bond stretching and OSiO angle bending, suggesting that the force constants associated with these displacements must be relatively large. On the otherhand, since the O atom typically vibrates with the greatest amplitude in the direction perpendicular to the SiOSi plane, the forces associated with the librational motions of the silicate groups are expected to be weak. Another important force present in SiO_2 polymorphs is the OO nonbonded repulsion forces between tetrahedra that have no atoms in common. It follows

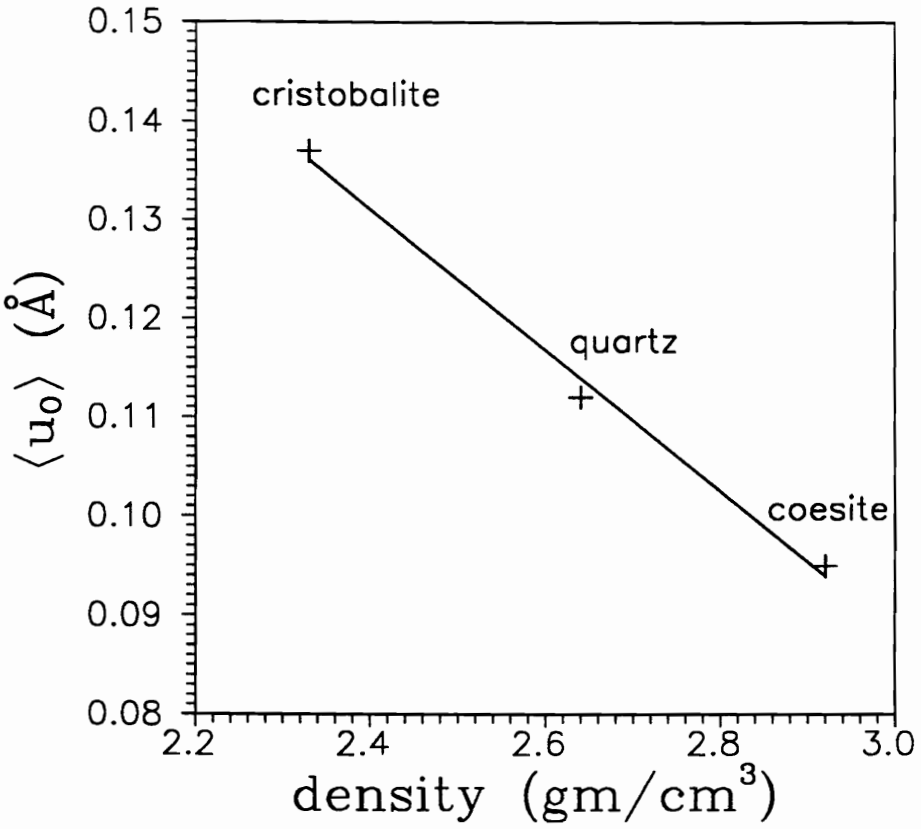

Figure 3–1. This plot demonstrates that the root–mean square displacement amplitudes of O, $\langle u_O \rangle$, are negatively correlated with the density of cristobalite, quartz (Kihara, 1990), and coesite (Geisinger et al. 1987, using the average of the 5 oxygens). A similar plot obtains for the Si atoms since the ratio of the displacements of O and Si are relatively constant for the silica polymorphs.

that the ease with which an atom in a framework structure can oscillate about its equilibrium position should depend, in part, on the packing density of the silicate tetrahedra. In fact, a plot of the average root–mean square displacement amplitudes, $< u_O >$, recorded for the O atoms in cristobalite, quartz and coesite show, as expected, that $< u_O >$ is negatively correlated with density (Figure 3–1). Not only may this explain the large thermal parameters reported for cristobalite, but it also suggests that the thermal parameters for the atoms in open high silica zeolite frameworks should also be relatively large. One may also ascribe the large thermal parameters observed for the feldspars to the low packing densities of their

tetrahedra.

High Pressure Cell Refinements

The crystal for which room pressure data were recorded was transferred to a diamond anvil cell (Merrill and Bassett, 1974) to record data at higher pressures. Using a 4:1 methanol to ethanol mixture as a pressure medium, the cell was mounted on an automated Picker four–circle diffractometer, using MoK_α radiation. The cell dimensions were refined with reflections ($30° \leq 2\theta \leq 52°$) that were recorded using the eight–reflection centering technique (King and Finger, 1979). The pressure calibration was completed by fitting Lorentzian functions to the fluorescence spectra of several small ruby chips which were included in the diamond anvil cell. Using least–squares estimates of the R_1 and R_2 peak positions, the pressure of the experiment was estimated using the relationship established by Piermarini et al. (1975). With this technique, pressure can be determined with a precision better than 0.01 GPa. Diffraction data were recorded at seven different pressures up to 1.60(4) GPa where the crystal transformed into a new, higher pressure structure type. A least–squares refinement of these data gave the cell dimensions in Table 3–1. The transformation occurred during data collection, several hours after a pressure of 1.60 GPa was obtained. The transformation took ~20 minutes to complete, based on the rate of diminution of the intensities being collected. Unfortunately, the crystal was lost when it was transferred to the Rigaku diffractometer for a study of its peak shapes.

A second crystal was selected and diffraction data were recorded at 18 pressures according to the sequence given in Table 3–1. During this sequence of experiments, the pressure was adjusted up and down several times. At 1.26 GPa, the crystal transformed to the high pressure phase, but it transformed back to α cristobalite upon lowering the pressure. Upon increasing the pressure, the crys-

tal transformed again to the high pressure structure type but at a slightly lower pressure (1.18 GPa). As with the first crystal, cell dimensions were refined with the data recorded at the pressures indicated in Table 3–1.

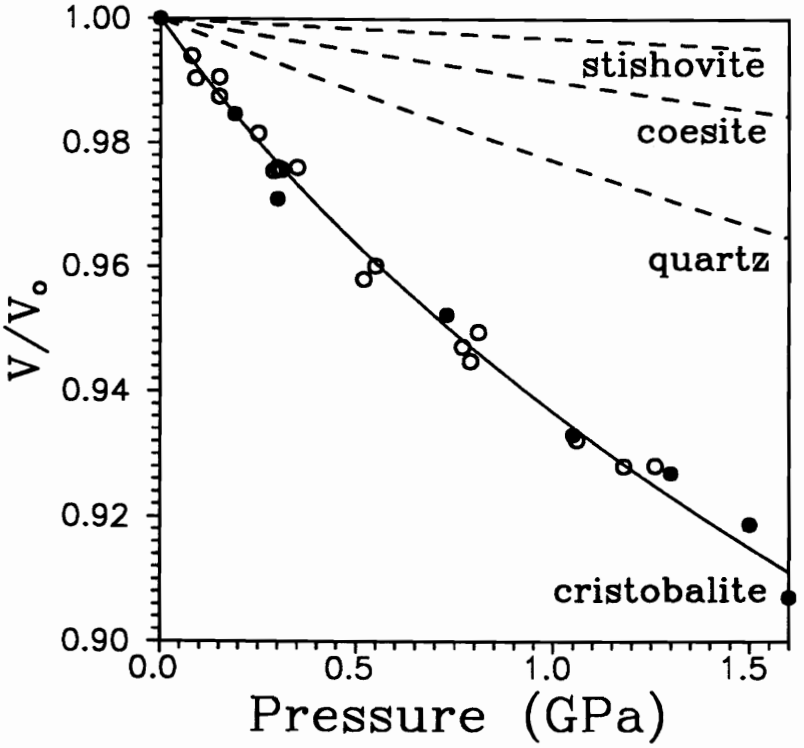

Figure 3–2. The unit cell volume of cristobalite as a function of pressure. The solid and open circles represent data from crystal 1 and crystal 2, respectively. The best fit Birch–Murnaghan equation of state (K_o = 11.5(7) GPa, K'_o = 9(2)) is represented as the solid curve. For comparison, the pressure–volume curves for quartz, coesite and stishovite are presented as dashed lines. This plot indicates that cristobalite is the most compressible of these SiO_2 polymorphs.

The unweighted volume, V/V_0, and pressure data recorded for the two crystals (Table 3–1) were fit to a Birch–Murnaghan equation of state according to the strategies proposed by Bass et al. (1981). These calculations yield a zero pressure bulk modulus of K_o=11.5(7) GPa with a pressure derivative of K'_o=9(2). The volume compressibility curve obtained in the analysis is displayed in Figure 3–2 along with the data recorded for the two crystals. The bulk modulus obtained in

this analysis is slightly smaller than that (16.4 GPa) determined in a recent Brillouin spectroscopic study (Yeganeh–Haeri et al. 1992) and that (18 GPa) reported by Tsuchida and Yagi (1990) obtained through an X–ray diffraction study of a powdered sample without using a hydrostatic medium in their high pressure cell. However, their study indicated that cristobalite transformed to a new structure at a pressure greater than 10 GPa, somewhat less than that (16.5 GPa) predicted by a molecular dynamics calculation (Tsuneyuki et al. 1989). On the other hand, Yeganeh–Haeri et al. (1990) determined the transformation pressure to be considerably lower, in conformity with the results obtained in this study. Perhaps, the transformation pressure obtained by Tsuchida and Yagi (1990) defines a transition to a different phase than the one reported here.

An examination of Figure 3–2 shows that cristobalite is much more compressible than quartz (K_o=41.4 GPa, K'_o=4; Glinnemann et al. 1992), coesite (K_o=95.4 GPa, K'_o=8.6; Levien and Prewitt, 1981) and stishovite (K_o=312.2 GPa, K'_o=1.8; Ross et al. 1990). The K'_o values obtained for these crystals range from 1.8 for stishovite to 9.0 for cristobalite with no apparent trends.

An examination of the cell dimensions (Table 3–1) reveals that the c–cell edge of cristobalite decreases at a faster rate than its a–cell edge (Figure 3–3). This shows that the cristobalite structure compresses at a faster rate along c than it does along a perpendicular direction. However, the converse is true in quartz where the c–cell edge decreases with increasing pressure at a slower rate than along a. These results are consistent with a modeling of the volume compressibilities which predicts that the cell edges in these two phases are conversely related with pressure as observed here (Boisen and Gibbs, submitted).

A linear regression of the cell edge data in Table 3–3 shows that the a and c cell edges are highly correlated with the c–cell edge compressing at a rate 2.07(2)

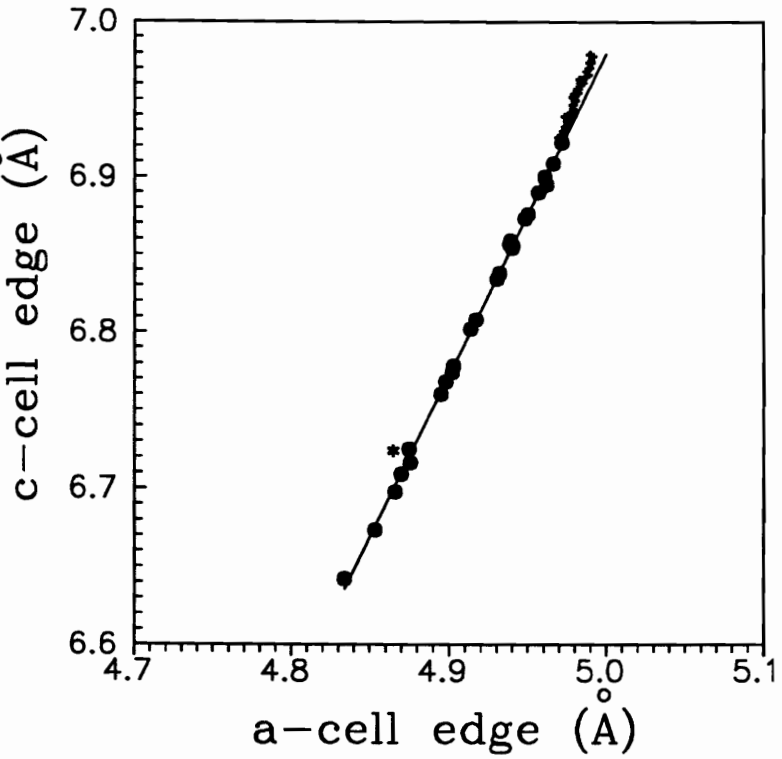

Figure 3–3. The variation of the c–cell edge versus the a–cell edge for cristobalite with data recorded at temperature (plus signs) and pressure (solid dots). The asterisk (*) represents the last data point for crystal 2 in Table 3–1 where the crystal underwent a phase transition during the data collection and may be considered to be an outlier. This plot shows that the relative effects of compression on the a– and c–cell edges remains constant over the pressure interval with c being 2 times more compressible than a. Furthermore, thermal expansion affects the two cell edges differently, as indicated by the change in slope.

times that of the a–cell edge. The cell edges recorded for cristobalite at high temperatures (Schmahl et al. 1992) are plotted on the figure for comparison. These data show a sharp break in the slope at ambient conditions, with the expansion rate of the c–cell edge 2.53(7) times that of the a–cell edge. This indicates that the structure expands upon heating at a faster rate along c relative to a than it compresses relative to a.

High Pressure Structure Refinements

Intensity data for the first crystal were recorded for a refinement of the structure up to $\sin\theta/\lambda = 0.7\text{Å}^{-1}$ at pressures of 0.19, 0.73 and 1.05 GPa on the automated Picker four–circle diffractometer with MoK_α radiation. A summary of the intensity collection procedures and refinement results is provided in Table 3–2. In particular, the value of the parameter, p, which is used to calculate the regression weights ($\sigma = \sqrt{\sigma_F^2 + p^2F^2}$), was assigned a value that constrained the calculated errors in the diffracted intensities to be normally distributed through a probability plot analysis according to the strategies of Abrahams and Keve (1971). All parameters varied smoothly with pressure, except for the isotropic temperature factor for the O atom. The structure was refined with an anisotropic temperature factor model; however, the resulting differences in the displacement parameters of Si and O did not indicate rigid body behavior of the silicate tetrahedra. It was concluded that the anisotropic temperature factors obtained at pressure did not provide a meaningful measure of the thermal motion and so the refinement was completed with an isotropic temperature factor model. Selected bond lengths and angles are found in Table 3–3.

Structural variations with pressure

With increasing pressure, the SiO_4 silicate tetrahedron in cristobalite undergoes a slight distortion. The SiO bond lengths remain unchanged while two of the OSiO angles show a small deviation from values observed at room pressure. The OSiO angle which lies more or less parallel to the c-axis is found to decrease by 0.4° while the one that lies more or less in the ab plane increases by 1°.

On the other hand, the SiOSi angle decreased by 6° over the 1.05 GPa pressure range. This is a significantly greater change than that observed for either quartz or coesite for the same pressure range. To appreciate the relative change in angle

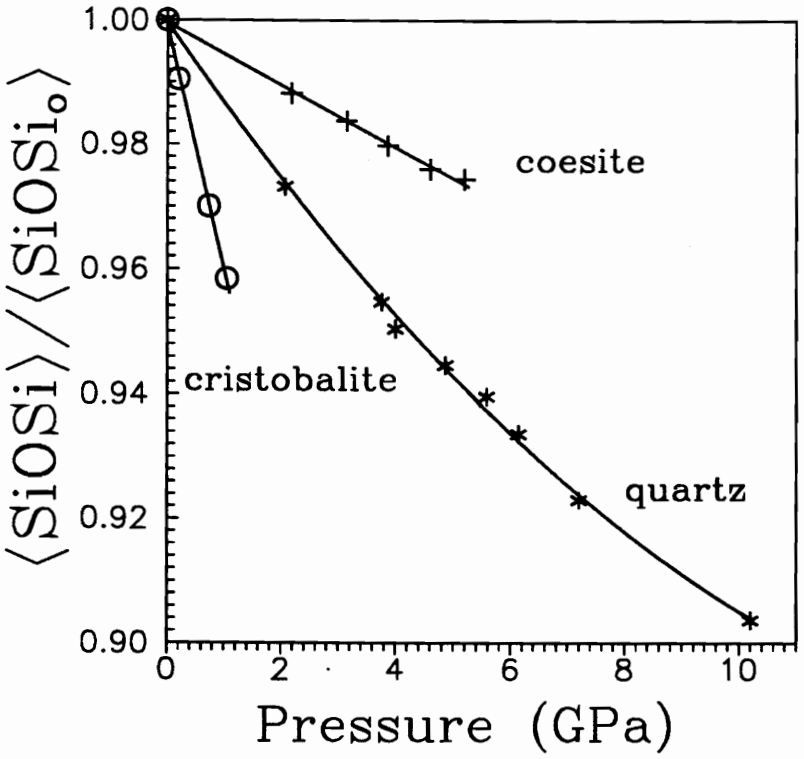

Figure 3–4a. Pressure plotted against the normalized average SiOSi angle observed for cristobalite, quartz (Levien et al. 1980; Glinnemann et al. 1992) and coesite (Levien and Prewitt, 1981). This figure demonstrates the different rates of compression for the normalized angles, with the rate equal to -0.039(1) GPa^{-1} for cristobalite, -0.0133(4) GPa^{-1} for quartz and -0.0050(1) GPa^{-1} for coesite.

in the three polymorphs, ϕ =<SiOSi> / <$SiOSi_0$ > was plotted as a function of pressure (Figure 3–4a) where <SiOSi> is the averaged SiOSi angle at pressure and <$SiOSi_0$ > is the average angle at room pressure. The trends of ϕ for the three polymorphs with pressure mirror that between V/V_0 and pressure (Figure 3–2). When ϕ is plotted against V/V_0 for all three polymorphs, the data fall along a single curve (Figure 3–4b) rather than three distinct curves as displayed in Figures 3–2 and 3–4a. The line drawn through the data in Figure 3–4b was calculated for both quartz and cristobalite, using a modified SQLOO energy function (Boisen and Gibbs, submitted). The details of this function are described in the Appendix.

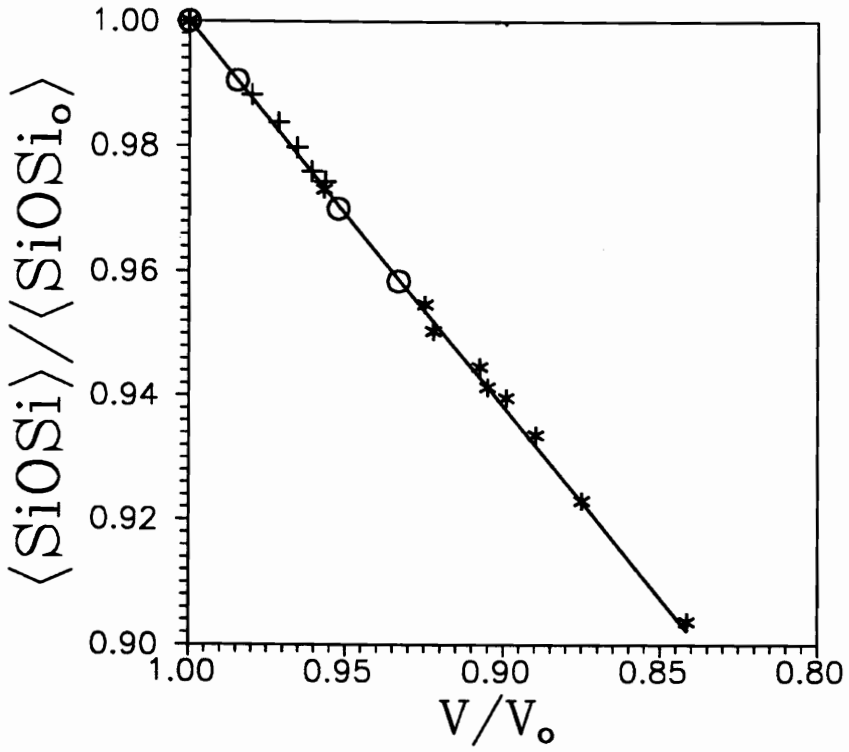

Figure 3–4b. A plot of the normalized unit cell volume, V/V_0, against the normalized average SiOSi angle observed for cristobalite, quartz and coesite. The symbols are the same as in Figure 3–4a. There are also two identical lines which represent the modeled variation for cristobalite and for quartz.

The fact that ϕ and V/V_0 are linearly correlated is not surprising in light of the correlations presented in Figures 3–2 and 3–4a. What is surprising is that ϕ versus V/V_0 data for all three polymorphs fall along a single straight line. This result suggests that the percentage decrease of the volume is directly proportional to the percentage decrease of the SiOSi angle, regardless of the framework structure type. The SQLOO calculations indicate that the total energy for a given change in volume compressiblity is larger for quartz than for cristobalite. On the other hand, the calculations also indicate that the contribution to the total energy ascribed to the SiOSi bending terms is the same. This can explain why the calculated lines for both quartz and cristobalite, superimposed in Figure 3–4b, lie upon each

other. Since the theoretical data fall along the same trend as the observed data, it appears that the SQLOO model provides an explaination of the trend.

Appendix

The configurational energy, E, of the unit cell was calculated with an expression based on the SQLOO model of Boisen and Gibbs, (submitted)

$$E = K_H \left\{ \sum^{SiO} k_R(R - R_0)^2 + \sum^{SiO \cdot SiO} k_{RR}(R_1 - R_{10})(R_2 - R_{20}) + \sum^{SiOSi} k_\phi(\phi - \phi_0)^2 + \sum^{SiO \cdot SiOSi} k_{R\phi}(\phi - \phi_0)(R - R_0) + \sum^{OSiO} k_\theta(\theta - \theta_0)^2 \right\} + K_{OO} \sum^{OO} \{e^{-cR(OO)} - e^{-R_0(OO)c}\},$$

where the terms are summed over all the SiO bond lengths, SiOSi and OSiO angles and the non–codimer OO separations in the unit cell. The regressor variables, R_0, ϕ_0 and θ_0 were assigned the room pressure values from this study for cristobalite, and the values from Levien et al. (1980) for quartz. The force constant parameters were modified from the values used by Boisen and Gibbs to give bond lengths and angles that matched, as closely as possible, the observed values for cristobalite at V=159.66 Å^3. These parameter values (Table 3–4) are very similar to quantum mechanical force constants derived by Boisen and Gibbs (submitted) obtained for the molecule $H_6Si_2O_7$. The close agreement with the force constants obtained here supports the assertion that molecules can serve as models for bonding in silicates (Gibbs, 1982).

Table 3–1. Cell parameters for cristobalite as a function of pressure.

Pressure (GPa)	a (Å)	c (Å)	Volume (Å^3)
crystal 1			
0.0	4.9717(4)	6.9223(3)	171.10(1)†
0.19(3)	4.9501(6)	6.8760(6)	168.48(4)†
0.30(3)	4.9304(8)	6.8343(8)	166.13(5)
0.73(3)	4.9028(8)	6.7782(9)	162.93(6)†
1.05(4)	4.8757(8)	6.7163(8)	159.66(6)†
1.30(3)	4.8662(8)	6.6979(7)	158.61(5)
1.50(4)	4.8535(8)	6.6733(8)	157.20(5)
1.60(4)	4.834(6)	6.642(2)	155.2(4) *
crystal 2			
0.0	4.975(1)	6.9259(8)	171.42(9)
0.08(3)	4.9662(8)	6.9087(9)	170.39(5)
0.15(9)	4.9608(9)	6.900(1)	169.81(6)
0.15(8)	4.9568(9)	6.890(1)	169.28(6)
0.25(8)	4.9482(9)	6.873(1)	168.27(6)
0.35(8)	4.9404(8)	6.8557(9)	167.33(6)
0.77(8)	4.898(1)	6.768(1)	162.37(6)
0.81(8)	4.902(1)	6.774(1)	162.78(7)
0.29(6)	4.9384(8)	6.8567(9)	167.22(5)
0.30(7)	4.939(1)	6.859(1)	167.31(6)
0.31(6)	4.940(1)	6.854(1)	167.26(7)
0.55(6)	4.917(1)	6.808(1)	164.60(6)
0.52(3)	4.9136(9)	6.8019(9)	164.22(6)
1.06(4)	4.875(1)	6.725(1)	159.82(7)
1.26(3)	4.870(1)	6.709(1)	159.12(7)*
0.09(4)	4.9620(8)	6.8951(9)	169.77(6)
0.79(2)	4.895(1)	6.760(1)	161.98(7)
1.18(3)	4.865(7)	6.724(7)	159.1(4) *

The data are presented in the order in which they were collected. The pressure was adjusted up and down several times for crystal 2. The crystals transformed to a new phase during the runs indicated with *. Intensity data were collected for the runs indicated with †.

Table 3–2. Intensity collection and refinement results for cristobalite as a function of pressure.

Pressure (GPa)	0.0001	0.19	0.73	1.05
No. obs. $I > 2\sigma_F$	146	106	105	102
$p^\dagger$	0.0	0.025	0.04	0.06
Weighted R	0.010	0.040	0.055	0.074
Unweighted R	0.029	0.053	0.056	0.065
u	0.30028(9)	0.3027(4)	0.3086(4)	0.3125(5)
B(Si)*	0.765(7)	0.80(4)	0.63(5)	0.51(7)
x	0.2392(2)	0.2388(8)	0.2364(10)	0.2356(15)
y	0.1044(2)	0.1086(9)	0.1198(11)	0.1269(15)
z	0.1787(1)	0.1817(5)	0.1870(6)	0.1904(8)
B(O)*	1.48(3)	1.22(9)	1.07(9)	1.12(12)

† Weights were computed by $\sigma = \sqrt{\sigma_F^2 + p^2 F^2}$.
* Values for B(Si) and B(O) at room pressure represent isotropic equivalents of the anisotropic temperature factors given by $\exp\{-\sum\sum h_j h_k \beta_{jk}\}$, where $\beta_{11} = \beta_{22} = 0.0077(1)$, $\beta_{33} = 0.00401(9)$, $\beta_{12} = -0.0003(2)$, $\beta_{13} = -\beta_{23} = 0.0008(1)$ for Si and $\beta_{11} = 0.0244(7)$, $\beta_{22} = 0.0086(5)$, $\beta_{33} = 0.0062(2)$, $\beta_{12} = -0.0013(4)$, $\beta_{13} = 0.0027(3)$, $\beta_{23} = 0.0005(3)$ for O.

Table 3–3. Selected interatomic distances (Å) and angles (°) for cristobalite.

Pressure (GPa)	0.0001	0.19	0.73	1.05
R(SiO) ×2 (Å)	1.603(1)	1.598(5)	1.600(6)	1.602(8)
R(SiO) ×2	1.603(1)	1.608(4)	1.609(5)	1.610(6)
SiOSi (°)	146.49(6)	145.1(2)	142.1(3)	140.4(4)
OSiO ×2	108.20(2)	108.2(1)	108.0(1)	107.8(2)
OSiO	109.03(9)	109.3(3)	109.6(4)	110.0(5)
OSiO ×2	109.99(7)	109.8(3)	109.9(3)	109.8(4)
OSiO	111.42(8)	111.6(3)	111.6(4)	111.6(5)

Table 3–4. Energy parameters (in atomic units) obtained for cristobalite.

Parameter	value
K_H	0.677687
k_R	0.30999
k_{RR}	0.04877
k_ϕ	0.15490
$k_{R\phi}$	0.127720
k_θ	1.43326
K_{OO}	590733.0
c	4.19058
$R_0(OO)$	7.5

References

Abrahams, S.C. and Keve, E.T. (1971) Normal probability plot analysis of error in measured and derived quantities and standard deviations. Acta Crystallographia, A27, 157-165.

Bass, J.D., Liebermann, R.C., Weidner, D.J. and Finch, S.J. (1981) Elastic properties from acoustic and volume compression experiments. Physics of the Earth and Planetary Interiors, 25, 140-158.

Becker, P.J. and Coppens, P. (1975) Extinction within the limit of validity of the Darwin transfer equations. III. Non–spherical crystals and anisotropy of extinction. Acta Crystallographia, A31, 417-425.

Boisen, M.B., Jr. and Gibbs, G.V. (1987) A method for calculating fractional s-character for bonds of tetrahedral oxyanions in crystals. Physics and Chemistry of Minerals, 14, 373-376.

Boisen, M.B., Jr., Gibbs, G.V., Downs, R.T. and D'Arco, P. (1990) The dependence of the SiO bond length on structural parameters in coesite, the silica polymorphs and the clathrasils. American Mineralogist, 75, 748-754.

Cheilikowsky, J.R., King, H.E., Jr., Troullier, N., Martins, J.L. and Glinnemann, J. (1990) Structural properties of $\alpha-$quartz near the amorphous transition. Physical Review Letters, 65, 3309-3312.

Dollase, W.A. (1965) Reinvestigation of the structure of low cristobalite. Zeitschrift für Kristallographie, 121, 369-377.

Downs, R.T., Gibbs, G.V. and Boisen, M.B.Jr. (1990) A study of the mean-square displacement amplitudes of Si, Al and O atoms in framework structures: Evidence for rigid bonds, order, twinning and stacking faults. American Mineralogist, 75, 1253-1267.

Finger, L.W. and Prince, E. (1965) A system of Fortran IV computer programs for crystal structure computations. United States National Bureau of Standards, Technical Note 854.

Geisinger, K.L., Spackman, M.A. and Gibbs, G.V. (1987) Exploration of structure, electron density distribution and bonding in coesite with Fourier and pseudoatom refinement methods using single-crystal X-ray diffraction data. The Journal of Physical Chemistry, 91, 3237-3244.

Gibbs, G.V. (1982) Molecules as models for bonding in silicates. American Mineralogist, 67, 421-450.

Gibbs, G.V., Boisen, M.B., Jr., Downs, R.T. and Lasaga, A.C. (1988) Mathematical Modeling of the structures and bulk moduli of TX_2 quartz and cristobalite structure types, T = C, Si, Ge and X = O, S. Materials Research Society Symposium Proceedings, 121, 155-165.

Glinnemann, J., King, H.E.Jr., Schulz, H., Hahn, Th., La Placa, S.J. and Dacol, F. (1992) Crystal structures of the low–temperature quartz–type phases of

SiO_2 and GeO_2 at elevated pressure. Zeitschrift für Kristallographie, 198, 177-212.

Hatch, D.M. and Ghose, S. (1991) The $\alpha-\beta$ phase transition in cristobalite, SiO_2. Physics and Chemistry of Minerals, 17, 554-562.

Hua, G.L., Welberry, T.R., Withers, R.L. and Thompson, J.G. (1988) An electron diffraction and lattice–dynamical study of the diffuse scattering in β–cristobalite, SiO_2. Journal of Applied Crystallography, 21, 458-465.

Kihara, K. (1990) An X-ray study of the temperature dependence of the quartz structure. European Journal of Mineralogy, 2, 63-77.

King, H.E. and Finger, L.W. (1979) Diffracted beam crystal centering and its application to high–pressure crystallography. Journal of Applied Crystallography, 12, 374-378.

Lasaga, A.C. and Gibbs, G.V. (1987) Applications of quantum mechanical potential surfaces to mineral physics calculations. Physics and Chemistry of Minerals, 14, 107-117.

Lasaga, A.C. and Gibbs, G.V. (1988) Quantum mechanical potential surfaces and calculations on minerals and molecular clusters I. STO–3G and 6–31G* results. Physics and Chemistry of Minerals, 16, 29-41.

Levien, L., Prewitt, C.T. and Weidner, D.J. (1980) Structure and elastic properties of quartz at pressure. American Mineralogist, 65, 920-930.

Levien, L. and Prewitt, C.T. (1981) High-pressure crystal structure and compressibility of coesite. American Mineralogist, 66, 324-333.

Merrill, L. and Bassett, W.A. (1974) Miniature diamond anvil pressure cell for single crystal X–ray diffraction studies. Review of Scientific Instruments, 45, 290-294.

Nieuwenkamp, W. (1937) Über die struktur von hoch–cristobalit. Zeitschrift für Kristallographie, 96, 454-458.

Peacor, D.R. (1973) High-temperature single-crystal study of the cristobalite inversion. Zeitschrift für Kristallographie, 138, 274-298.

Piermarini, G.J., Block, S., Barnett, J.D. and Forman, R.A. (1975) Calibration of the pressure dependence of the R_1 ruby fluorescence line to 195 kbar. Journal of Applied Crystallography, 46, 2774-2780.

Pluth, J.J., Smith, J.V. and Faber, J., Jr. (1985) Crystal structure of low cristobalite at 10, 293 and 473 K: Variation of framework geometry with temperature. The Journal of Applied Physics, 57, 1045-1049.

Ross, N., Shu, J-F., Hazen, R.M. and Gasparik, T. (1990) High–pressure crystal chemistry of stishovite. American Mineralogist, 75, 739-747.

Sanders, M.L., Leslie, M. and Catlow, C.R.A. (1984) Interatomic potentials for

SiO_2. The Journal of the Chemical Society, Chemical Communications, 1271-1273.

Schmahl, W.W., Swainson, I.P., Dove, M.T. and Graeme–Barber, A. (1992) Landau free energy and order parameter behaviour of the α/β phase transition in cristobalite. Zeitschrift für Kristallographie, 201, 125-145.

Stixrude, L. and Bukowinski, M.S.T. (1988) Simple covalent potential models of tetrahedral SiO_2: Applications to α–quartz and coesite at pressure. Physics and Chemistry of Minerals, 16, 199-206.

Tsuchida, Y. and Yagi, T. (1990) New pressure–induced transformations of silica at room temperature. Nature, 347, 267-269.

Tsuneyuki, S., Tsukada, M., Aoki, H. and Matsui, Y. (1988) First–principles interatomic potentials of silica applied to molecular dynamics. Physical Review Letters, 61, 869-872.

Tsuneyuki, S., Matsui, Y., Aoki, H. and Tsukada, M. (1989) New pressure–induced structural transformations in silica obtained by computer simulation. Nature, 339, 209-211.

van Beest, B.W.H., Kramer, G.J. and van Santen, R.A. (1990) Force fields for silicas and aluminophosphates based on *ab initio* calculations. Physical Review Letters, 64, 1955-1958.

Van Valkenburg, A.Jr. and Buie, B.F. (1945) Octahedral cristobalite with quartz paramorphs from Ellora Caves, Hyderabad State, India. American Mineralogist, 30, 526-535.

Yeganeh–Haeri, A., Weidner, D.J., Parise, J., Ko, J., Vaughan, M.T., Liu, X., Zhao, Y., Wang, Y. and Pacalo, R. (1990) A new polymorph of SiO_2. Transactions of the American Geophysical Union, 71, 1671.

Yeganeh–Haeri, A., Weidner, D.J. and Parise, J.B. (1992) Elasticity of α–cristobalite: A silicon dioxide with a negative Poisson's ratio. Science, 257, 650-652.

Appendix

Observed and Calculated Structure Factors

for Cristobalite at Room Pressure

H	K	L	|Fo|	|Fc|	σF	EXTIN
2	0	0	46.636	45.029	.133	0.9997*
4	0	0	6.884	6.491	.315	1.0000
6	0	0	0.948	1.795	4.554	1.0000* **
1	1	0	6.867	6.842	.158	1.0000
2	1	0	2.164	0.485	.420	1.0000
3	1	0	10.227	9.915	.206	1.0000
4	1	0	26.066	26.190	.212	1.0000
5	1	0	7.330	7.078	.335	1.0000
6	1	0	17.595	17.378	.298	1.0000
2	2	0	13.006	13.038	.179	1.0000
3	2	0	0.695	1.054	3.475	1.0000* **
4	2	0	3.673	3.282	.520	1.0000
5	2	0	3.662	3.863	.622	1.0000
6	2	0	2.442	1.172	1.614	1.0000
3	3	0	17.455	17.702	.232	1.0000
4	3	0	15.848	16.118	.264	1.0000
5	3	0	13.231	13.381	.315	1.0000
6	3	0	11.413	11.209	.365	1.0000
4	4	0	6.327	6.586	.411	1.0000
5	4	0	0.873	1.945	4.364	1.0000* **
1	0	1	50.328	50.314	.098	0.9995
2	0	1	4.371	2.982	.216	1.0000*
3	0	1	29.699	28.573	.171	0.9999*
4	0	1	22.185	22.328	.213	1.0000
5	0	1	4.473	4.550	.506	1.0000
6	0	1	15.003	14.873	.311	1.0000
1	1	1	19.967	19.905	.127	0.9999
2	1	1	12.029	12.411	.169	1.0000
3	1	1	18.310	18.209	.191	1.0000
4	1	1	7.904	8.006	.303	1.0000
5	1	1	10.199	10.256	.305	1.0000
6	1	1	4.445	4.239	.605	1.0000
2	2	1	4.314	3.833	.254	1.0000
3	2	1	13.743	13.665	.221	1.0000

* signifies that the reflection was rejected on the basis that $I < 2\ \sigma F$.

** signifies that the reflection has an intensity less than the minimum observable value.

H	K	L	|Fo|	|Fc|	σF	EXTIN	
4	2	1	16.304	16.569	.240	1.0000	
5	2	1	6.755	6.730	.387	1.0000	
6	2	1	12.288	11.954	.338	1.0000	
3	3	1	14.969	15.042	.242	1.0000	
4	3	1	11.926	12.058	.287	1.0000	
5	3	1	6.546	6.480	.419	1.0000	
6	3	1	8.096	8.028	.419	1.0000	
4	4	1	7.244	7.626	.388	1.0000	
5	4	1	9.271	9.165	.387	1.0000	
1	0	2	25.388	24.735	.129	0.9999*	
2	0	2	18.176	16.820	.157	1.0000*	
3	0	2	27.915	28.046	.184	0.9999	
4	0	2	11.678	11.638	.244	1.0000	
5	0	2	16.353	16.203	.266	1.0000	
6	0	2	0.852	1.100	4.254	1.0000*	**
1	1	2	17.050	17.844	.143	1.0000*	
2	1	2	20.438	19.734	.165	1.0000	
3	1	2	18.936	18.713	.195	1.0000	
4	1	2	6.897	7.033	.319	1.0000	
5	1	2	1.916	1.857	1.599	1.0000*	**
6	1	2	3.504	3.597	.995	1.0000	
2	2	2	8.609	8.632	.226	1.0000	
3	2	2	21.141	21.209	.210	1.0000	
4	2	2	12.292	12.369	.267	1.0000	
5	2	2	11.163	11.342	.316	1.0000	
6	2	2	8.216	8.377	.411	1.0000	
3	3	2	16.338	16.515	.241	1.0000	
4	3	2	5.820	5.716	.376	1.0000	
5	3	2	4.090	2.702	.811	1.0000	
6	3	2	3.443	2.767	.999	1.0000	
4	4	2	15.564	15.734	.299	1.0000	
5	4	2	2.527	1.533	1.880	1.0000*	**
1	0	3	3.462	4.008	.238	1.0000	
2	0	3	22.790	22.340	.174	1.0000	
3	0	3	15.297	15.284	.205	1.0000	
4	0	3	14.652	14.514	.244	1.0000	
5	0	3	0.796	1.106	3.904	1.0000*	**
6	0	3	8.508	8.694	.404	1.0000	
1	1	3	27.518	26.688	.157	0.9999*	
2	1	3	11.822	11.623	.199	1.0000	
3	1	3	20.799	20.819	.206	1.0000	
4	1	3	6.079	6.121	.322	1.0000	
5	1	3	8.174	8.041	.348	1.0000	
6	1	3	7.357	7.103	.440	1.0000	
2	2	3	21.373	21.354	.194	1.0000	
3	2	3	17.604	17.668	.223	1.0000	
4	2	3	10.738	10.694	.279	1.0000	

H	K	L	|Fo|	|Fc|	σF	EXTIN	
5	2	3	6.872	6.728	.388	1.0000	
6	2	3	5.868	5.543	.527	1.0000	
3	3	3	11.966	11.992	.272	1.0000	
4	3	3	13.025	13.212	.299	1.0000	
5	3	3	0.875	1.715	4.373	1.0000*	**
4	4	3	2.350	2.204	1.631	1.0000	
5	4	3	9.704	9.923	.405	1.0000	
0	0	4	24.788	24.869	.166	1.0000	
1	0	4	10.293	10.096	.206	1.0000	
2	0	4	21.035	21.084	.195	1.0000	
3	0	4	1.882	1.856	1.688	1.0000*	**
4	0	4	6.710	6.635	.324	1.0000	
5	0	4	7.293	6.884	.386	1.0000	
6	0	4	5.184	5.548	.535	1.0000	
1	1	4	2.676	2.101	.331	1.0000	
2	1	4	20.218	19.982	.200	1.0000	
3	1	4	13.998	14.125	.233	1.0000	
4	1	4	18.926	18.778	.249	1.0000	
5	1	4	6.082	5.971	.456	1.0000	
6	1	4	12.069	11.784	.360	1.0000	
2	2	4	17.662	17.721	.219	1.0000	
3	2	4	9.139	9.166	.289	1.0000	
4	2	4	6.078	6.244	.413	1.0000	
5	2	4	5.294	4.806	.570	1.0000	
6	2	4	4.636	4.140	.695	1.0000	
3	3	4	12.734	12.702	.283	1.0000	
4	3	4	8.592	8.658	.353	1.0000	
5	3	4	12.004	11.935	.353	1.0000	
4	4	4	2.952	2.465	1.060	1.0000	
1	0	5	26.176	26.028	.195	1.0000	
2	0	5	8.043	7.876	.284	1.0000	
3	0	5	3.010	2.513	.844	1.0000	
4	0	5	11.474	11.511	.306	1.0000	
5	0	5	1.729	0.666	2.841	1.0000*	**
6	0	5	8.120	7.841	.443	1.0000	
1	1	5	3.401	3.335	.386	1.0000	
2	1	5	18.376	18.693	.219	1.0000	
3	1	5	9.796	9.656	.278	1.0000	
4	1	5	6.957	7.090	.410	1.0000	
5	1	5	15.647	15.574	.311	1.0000	
2	2	5	9.364	9.489	.277	1.0000	
3	2	5	8.046	8.033	.317	1.0000	
4	2	5	9.852	9.933	.338	1.0000	
5	2	5	7.439	7.464	.453	1.0000	
3	3	5	6.491	5.834	.405	1.0000	
4	3	5	8.407	8.338	.374	1.0000	
5	3	5	8.958	8.979	.412	1.0000	

H	K	L	|Fo|	|Fc|	σF	EXTIN	
4	4	5	5.677	5.090	.549	1.0000	
1	0	6	2.230	0.636	1.149	1.0000	
2	0	6	4.063	3.715	.404	1.0000	
3	0	6	12.506	12.338	.287	1.0000	
4	0	6	4.115	3.544	.650	1.0000	
5	0	6	16.765	16.754	.324	1.0000	
1	1	6	28.988	29.455	.219	1.0000	
2	1	6	3.594	3.420	.435	1.0000	
3	1	6	8.274	8.303	.327	1.0000	
4	1	6	0.832	1.294	4.166	1.0000*	**
5	1	6	0.896	0.933	4.524	1.0000*	**
2	2	6	8.975	8.803	.316	1.0000	
3	2	6	10.475	10.434	.327	1.0000	
4	2	6	9.530	9.561	.363	1.0000	
5	2	6	14.160	14.159	.323	1.0000	
3	3	6	0.848	2.052	4.183	1.0000*	**
4	3	6	4.377	3.170	.768	1.0000	
1	0	7	11.450	11.709	.293	1.0000	
2	0	7	11.358	11.426	.312	1.0000	
3	0	7	0.828	0.322	4.137	1.0000*	**
4	0	7	7.589	7.214	.409	1.0000	
1	1	7	0.805	0.724	4.010	1.0000*	**
2	1	7	13.191	13.443	.297	1.0000	
3	1	7	7.841	7.657	.390	1.0000	
4	1	7	7.366	7.288	.455	1.0000	
2	2	7	13.823	13.896	.304	1.0000	
3	2	7	6.774	6.726	.431	1.0000	
4	2	7	8.269	8.009	.414	1.0000	
3	3	7	4.931	4.507	.674	1.0000	
0	0	8	7.438	7.429	.391	1.0000	
1	0	8	2.339	1.658	1.877	1.0000*	**
2	0	8	9.653	9.655	.408	1.0000	
3	0	8	0.879	0.167	4.395	1.0000*	**
4	0	8	5.022	4.085	.705	1.0000	
1	1	8	1.566	1.260	2.713	1.0000*	**
2	1	8	13.331	13.296	.317	1.0000	
3	1	8	3.903	3.826	.822	1.0000	
2	2	8	11.175	11.408	.350	1.0000	
3	2	8	7.830	7.527	.425	1.0000	
1	0	9	5.206	4.879	.536	1.0000	
2	0	9	9.732	9.663	.395	1.0000	
1	1	9	5.294	4.973	.494	1.0000	
2	1	9	8.154	7.982	.450	1.0000	

Observed and Calculated Structure Factors for Cristobalite at 0.19 GPa

H	K	L	|Fo|	|Fc|	σF	
2	0	0	47.450	46.325	1.191	
4	0	0	4.731	6.603	1.201	
6	0	0	3.591	0.948	2.689*	**
2	1	0	2.098	0.144	2.466*	**
3	1	0	10.997	10.782	.421	
4	1	0	44.930	24.807	1.144*	
5	1	0	7.505	7.780	.784	
6	1	0	16.402	16.089	.574	
5	2	0	3.171	6.250	2.115	
1	0	1	51.101	49.774	1.280	
2	0	1	3.896	1.776	.906	
3	0	1	28.294	28.835	.729	
4	0	1	20.752	21.698	.576	
5	0	1	3.372	5.263	3.064*	**
6	0	1	14.912	14.567	.586	
1	1	1	19.921	20.652	.519	
2	1	1	12.582	12.434	.392	
3	1	1	18.143	18.652	.512	
4	1	1	9.889	9.300	.515	
5	1	1	10.384	9.716	.602	
6	1	1	3.967	5.401	2.556	
3	2	1	13.283	13.624	.443	
4	2	1	14.774	15.868	.485	
5	2	1	5.919	6.678	1.348	
6	2	1	16.912	12.182	.621*	
1	0	2	25.900	25.774	.661	
2	0	2	17.345	16.206	.486	
3	0	2	30.042	29.769	.774	
4	0	2	12.258	12.599	.508	
5	0	2	16.448	16.813	.544	
6	0	2	5.541	1.176	2.285	
1	1	2	14.960	16.078	.417	
2	1	2	20.584	20.011	.548	
3	1	2	17.307	16.650	.491	
4	1	2	7.409	6.741	.668	
5	1	2	3.251	3.263	3.158*	**
6	1	2	4.483	3.755	2.296	
2	2	2	9.395	8.820	.419	
3	2	2	21.352	21.543	.583	
4	2	2	12.229	12.625	.482	

H	K	L	|Fo|	|Fc|	σF	
5	2	2	10.168	10.895	.603	
6	2	2	8.839	7.467	.710	
1	0	3	2.610	4.039	2.016*	**
2	0	3	22.305	22.323	.606	
3	0	3	14.771	13.773	.487	
4	0	3	15.660	15.931	.510	
5	0	3	2.028	2.398	4.793*	**
6	0	3	8.596	9.124	.819	
1	1	3	28.275	27.169	.724	
2	1	3	10.518	10.011	.411	
3	1	3	21.721	21.951	.591	
4	1	3	5.836	5.207	1.342	
5	1	3	8.278	8.419	.776	
6	1	3	7.858	7.629	.833	
2	2	3	19.811	20.660	.551	
3	2	3	16.345	16.803	.497	
4	2	3	10.755	10.461	.514	
5	2	3	6.724	6.120	.886	
6	2	3	3.772	4.816	2.525	
0	0	4	26.786	26.959	.689	
1	0	4	10.438	9.926	.422	
2	0	4	20.592	20.672	.563	
3	0	4	2.611	2.248	2.725*	**
4	0	4	5.381	4.998	1.373	
5	0	4	5.801	6.868	2.586	
6	0	4	7.024	6.266	1.087	
1	1	4	3.439	2.913	1.955	
2	1	4	19.474	19.654	.542	
3	1	4	13.813	14.547	.482	
4	1	4	18.803	19.196	.555	
5	1	4	6.377	6.824	1.040	
6	1	4	11.224	11.246	.671	
2	2	4	16.165	16.235	.483	
3	2	4	8.977	9.222	.546	
4	2	4	2.786	5.032	3.011*	**
5	2	4	5.188	4.182	1.854	
6	2	4	2.582	4.518	4.257*	**
1	0	5	26.811	26.789	.712	
2	0	5	7.587	7.603	.582	
3	0	5	2.314	3.414	3.936*	**
4	0	5	11.914	11.637	.544	
5	0	5	2.509	1.228	3.660*	**
1	1	5	2.727	3.117	3.228*	**
2	1	5	18.537	18.309	.535	
3	1	5	9.832	8.998	.536	
4	1	5	5.276	6.747	1.772	
5	1	5	15.169	14.497	.574	

H	K	L	|Fo|	|Fc|	σF	
2	2	5	9.045	8.977	.637	
3	2	5	9.639	8.745	.641	
4	2	5	9.653	10.028	.635	
5	2	5	7.548	7.607	.905	
1	0	6	1.926	1.617	4.126*	**
2	0	6	3.846	4.723	1.645	
3	0	6	12.072	12.567	.521	
4	0	6	2.522	5.139	3.421*	**
5	0	6	15.694	15.555	.567	
1	1	6	28.486	28.702	.746	
2	1	6	4.510	3.538	3.123	
3	1	6	7.328	8.292	.735	
4	1	6	2.070	2.213	4.557*	**
5	1	6	2.221	0.745	4.800*	**
2	2	6	9.950	8.929	.607	
3	2	6	9.980	10.132	.622	
4	2	6	10.162	9.923	.672	
5	2	6	12.540	13.136	.607	
3	3	6	2.463	2.488	3.676*	**
4	3	6	4.405	1.895	1.603	
1	0	7	10.942	10.532	.515	
2	0	7	12.161	12.121	.523	
3	0	7	2.052	0.438	4.670*	**
4	0	7	7.952	7.550	.791	
1	1	7	2.832	2.093	3.560*	**
2	1	7	12.681	12.796	.547	
3	1	7	8.380	8.153	.715	
4	1	7	8.091	7.241	.824	
2	2	7	14.073	14.059	.512	
3	2	7	6.045	6.469	1.470	
4	2	7	10.982	7.470	.904	
3	3	7	3.751	3.706	2.601	
1	0	8	1.818	1.057	4.606*	**
2	0	8	8.898	8.587	.750	
3	0	8	2.067	0.306	4.911*	**
1	1	8	1.901	1.182	4.681*	**
2	1	8	13.107	13.619	.553	
3	1	8	4.799	3.419	2.265	
2	2	8	10.598	10.513	.620	
3	2	8	6.351	7.431	1.957	
1	0	9	6.866	5.097	1.080	
2	0	9	10.487	9.388	.587	
1	1	9	3.642	4.083	3.787*	**
2	1	9	7.557	7.676	.880	

Observed and Calculated Structure Factors

for Cristobalite at 0.73 GPa

H	K	L	|Fo|	|Fc|	σF	
2	0	0	49.381	47.484	1.978	
4	0	0	2.569	2.043	3.552*	**
6	0	0	7.065	4.462	1.142	
2	1	0	0.885	0.793	4.423*	**
3	1	0	13.097	12.950	.604	
4	1	0	20.972	22.577	.874	
5	1	0	8.535	8.724	.808	
6	1	0	16.035	15.454	.768	
1	0	1	50.729	47.873	2.031	
2	0	1	0.874	0.119	4.375*	**
3	0	1	26.276	26.404	1.072	
4	0	1	19.541	20.395	.824	
5	0	1	1.268	3.320	5.823*	**
6	0	1	14.915	14.904	.725	
1	1	1	20.919	21.621	.854	
2	1	1	13.272	13.460	.584	
3	1	1	19.459	20.107	.816	
4	1	1	12.427	12.335	.625	
5	1	1	9.674	9.207	.717	
6	1	1	7.833	8.342	.974	
3	2	1	13.841	14.792	.627	
4	2	1	13.752	14.545	.658	
5	2	1	7.094	7.224	.933	
6	2	1	13.697	13.174	.711	
1	0	2	28.564	27.571	1.152	
2	0	2	14.800	13.368	.630	
3	0	2	33.322	34.112	1.348	
4	0	2	12.033	12.347	.600	
5	0	2	16.671	17.593	.743	
6	0	2	1.823	2.360	5.028*	**
1	1	2	11.654	12.422	.500	
2	1	2	20.621	20.041	.850	
3	1	2	13.865	12.915	.610	
4	1	2	5.949	5.001	1.041	
5	1	2	4.356	5.384	1.588	
6	1	2	5.697	4.651	1.460	
2	2	2	10.880	10.356	.526	
3	2	2	23.073	23.309	.952	
4	2	2	13.789	14.236	.658	
5	2	2	10.192	10.611	.676	

H	K	L	|Fo|	|Fc|	σF	
6	2	2	6.791	6.978	1.010	
1	0	3	0.927	4.143	4.633*	**
2	0	3	23.516	22.961	.965	
3	0	3	13.598	12.376	.618	
4	0	3	17.668	18.425	.775	
5	0	3	1.222	2.513	6.107*	**
6	0	3	7.246	8.899	.979	
1	1	3	29.652	27.931	1.201	
2	1	3	7.627	7.467	.538	
3	1	3	23.997	24.551	.990	
4	1	3	3.707	5.110	1.621	
5	1	3	8.541	8.458	.783	
6	1	3	9.402	9.104	.803	
2	2	3	19.797	20.133	.822	
3	2	3	14.666	14.906	.654	
4	2	3	11.801	10.853	.613	
5	2	3	6.297	6.292	1.190	
6	2	3	4.086	4.770	2.142*	**
0	0	4	31.886	31.273	1.286	
1	0	4	9.835	9.144	.513	
2	0	4	20.747	20.853	.862	
3	0	4	2.267	3.537	3.806*	**
4	0	4	1.167	2.089	5.832*	**
5	0	4	1.241	6.708	6.206*	**
6	0	4	9.139	8.446	.783	
1	1	4	3.258	3.850	1.603	
2	1	4	19.003	19.319	.802	
3	1	4	14.985	14.988	.625	
4	1	4	19.589	20.197	.838	
5	1	4	9.858	8.814	.774	
6	1	4	10.694	10.655	.760	
2	2	4	14.454	14.113	.651	
3	2	4	8.863	8.590	.641	
4	2	4	1.183	2.690	5.917*	**
5	2	4	4.453	4.774	1.569	
1	0	5	28.272	28.763	1.150	
2	0	5	6.618	7.073	.743	
3	0	5	2.907	4.382	3.551*	**
4	0	5	11.985	11.973	.635	
5	0	5	3.966	4.027	2.919*	**
1	1	5	1.120	1.256	5.422*	**
2	1	5	17.845	18.273	.771	
3	1	5	8.628	8.488	.711	
4	1	5	4.364	5.884	1.560	
5	1	5	13.509	13.652	.736	
2	2	5	8.826	7.496	.633	
3	2	5	10.965	10.627	.645	

H	K	L	|Fo|	|Fc|	σF	
4	2	5	10.453	9.602	.697	
5	2	5	9.320	9.429	.774	
1	0	6	4.124	3.636	1.383	
2	0	6	5.104	5.451	1.228	
3	0	6	12.448	13.655	.651	
4	0	6	7.143	7.091	1.159	
5	0	6	14.193	14.950	.755	
1	1	6	27.195	28.047	1.115	
2	1	6	4.710	4.910	1.456	
3	1	6	6.961	7.664	.880	
4	1	6	1.336	2.088	6.006*	**
5	1	6	5.978	3.537	2.777	
2	2	6	11.410	10.741	.664	
3	2	6	10.751	10.435	.678	
4	2	6	12.292	11.960	.715	
3	3	6	2.912	2.116	3.254*	**
4	3	6	3.247	0.440	3.684*	**
1	0	7	9.187	9.223	.651	
2	0	7	13.483	14.167	.686	
3	0	7	1.208	0.903	6.052*	**
4	0	7	9.059	9.306	.827	
1	1	7	3.878	4.527	5.337*	**
2	1	7	11.344	11.384	.658	
3	1	7	9.994	9.384	.773	
4	1	7	6.769	6.634	1.078	
2	2	7	14.829	15.674	.706	
3	2	7	8.404	7.157	.807	
4	2	7	9.429	8.043	.790	
3	3	7	2.356	3.109	6.137*	**
1	0	8	5.080	0.082	1.687	
2	0	8	7.991	7.408	.980	
3	0	8	2.294	0.040	3.616*	**
1	1	8	1.259	1.539	6.292*	**
2	1	8	14.788	15.311	.735	
3	1	8	7.097	3.566	1.049	
2	2	8	8.470	8.762	.866	
3	2	8	7.345	7.512	1.050	
1	0	9	8.187	6.464	.898	
2	0	9	11.583	10.022	.712	
1	1	9	4.750	3.476	1.740	
2	1	9	9.092	7.950	.842	

Observed and Calculated Structure Factors

for Cristobalite at 1.05 GPa

H	K	L	|Fo|	|Fc|	σF	
2	0	0	49.812	48.033	2.989	
4	0	0	4.162	0.602	1.790	
6	0	0	9.642	8.306	.737	
2	1	0	2.071	1.698	3.169*	**
3	1	0	13.666	14.170	.843	
4	1	0	19.745	20.993	1.203	
5	1	0	9.369	9.105	.698	
6	1	0	16.045	14.130	1.008	
1	0	1	49.309	46.590	2.960	
2	0	1	2.256	1.331	3.025*	**
3	0	1	24.474	24.385	1.483	
4	0	1	18.618	19.312	1.138	
5	0	1	2.872	1.725	3.695*	**
6	0	1	14.125	14.093	.922	
1	1	1	21.689	22.188	1.306	
2	1	1	14.548	14.047	.885	
3	1	1	19.619	20.930	1.189	
4	1	1	13.893	13.847	.866	
5	1	1	10.777	9.078	.749	
6	1	1	11.848	10.513	.817	
3	2	1	14.287	15.542	.882	
4	2	1	12.474	13.698	.804	
5	2	1	5.430	7.648	1.725	
1	0	2	29.478	28.502	1.772	
2	0	2	12.765	11.575	.788	
3	0	2	36.174	36.539	2.175	
4	0	2	10.741	11.608	.711	
5	0	2	16.217	18.085	1.011	
6	0	2	1.405	3.012	7.024*	**
1	1	2	9.833	10.200	.616	
2	1	2	20.534	19.823	1.243	
3	1	2	11.559	10.150	.734	
4	1	2	3.451	3.680	4.305*	**
5	1	2	6.150	6.886	1.307	
6	1	2	5.655	4.973	2.296	
2	2	2	11.250	11.651	.717	
3	2	2	23.808	24.094	1.439	
4	2	2	15.090	12.128	.929	
5	2	2	9.551	10.542	.715	
6	2	2	5.537	6.617	1.834	

H	K	L	|Fo|	|Fc|	σF	
1	0	3	2.548	4.429	3.120*	**
2	0	3	23.618	23.094	1.425	
3	0	3	12.120	11.009	.767	
4	0	3	18.950	19.532	1.161	
5	0	3	2.006	2.901	6.674*	**
6	0	3	10.332	8.592	.749	
1	1	3	29.689	28.034	1.787	
2	1	3	8.346	6.491	.571	
3	1	3	25.268	25.803	1.526	
4	1	3	9.147	6.085	.672	
5	1	3	8.789	8.763	.714	
6	1	3	8.972	9.988	.761	
2	2	3	18.686	19.561	1.138	
3	2	3	13.359	13.851	.838	
4	2	3	10.422	11.082	.722	
5	2	3	5.405	6.426	3.703*	**
6	2	3	2.015	5.609	5.557*	**
0	0	4	34.638	33.972	2.084	
1	0	4	9.758	8.470	.635	
2	0	4	20.741	21.094	1.258	
3	0	4	3.485	4.206	2.054*	**
4	0	4	1.298	0.020	6.491*	**
5	0	4	5.932	5.839	2.527	
6	0	4	10.782	10.162	.807	
1	1	4	5.632	4.525	1.659	
2	1	4	18.914	18.978	1.153	
3	1	4	14.991	14.922	.940	
4	1	4	19.722	20.329	1.208	
5	1	4	11.147	9.677	.830	
6	1	4	9.741	9.963	.772	
2	2	4	13.212	13.078	.827	
3	2	4	8.308	7.990	.672	
4	2	4	3.184	2.142	3.423*	**
5	2	4	4.940	5.744	4.134*	**
1	0	5	29.285	29.572	1.763	
2	0	5	8.739	7.094	.641	
3	0	5	4.571	5.060	2.094	
4	0	5	11.316	12.020	.761	
5	0	5	6.525	5.644	1.287	
1	1	5	1.209	0.279	6.043*	**
2	1	5	18.119	18.194	1.116	
3	1	5	10.749	8.492	.738	
4	1	5	3.500	6.003	3.487*	**
5	1	5	11.773	12.566	.825	
2	2	5	6.945	6.674	.725	
3	2	5	11.293	11.738	.770	
4	2	5	9.336	9.092	.726	

H	K	L	|Fo|	|Fc|	σF	
5	2	5	10.272	10.294	.789	
1	0	6	8.380	5.193	.667	
2	0	6	6.126	5.446	.949	
3	0	6	13.482	14.906	.871	
4	0	6	7.605	7.722	.725	
5	0	6	14.461	14.308	.940	
1	1	6	26.416	27.140	1.597	
2	1	6	6.391	5.637	.864	
3	1	6	6.121	7.111	.734	
4	1	6	4.306	1.932	2.317*	**
5	1	6	4.893	5.543	4.873*	**
2	2	6	11.452	11.814	.821	
3	2	6	11.251	10.739	.808	
4	2	6	13.161	13.080	.871	
3	3	6	1.948	1.523	5.196*	**
1	0	7	8.784	8.657	.667	
2	0	7	14.506	15.165	.925	
3	0	7	1.319	0.907	6.948*	**
4	0	7	10.031	10.726	.770	
1	1	7	6.168	6.149	1.073	
2	1	7	9.400	10.261	.735	
3	1	7	10.543	10.443	.760	
4	1	7	6.010	5.732	1.485	
2	2	7	15.921	16.092	1.002	
3	2	7	9.343	7.609	.756	
4	2	7	10.327	8.251	.788	
3	3	7	3.367	3.116	3.127*	**
1	0	8	5.285	0.451	1.718	
2	0	8	7.158	7.038	.799	
3	0	8	1.389	0.287	6.948*	**
1	1	8	3.219	1.917	3.786*	*
2	1	8	15.675	15.937	.997	
3	1	8	6.078	4.306	1.966	
2	2	8	6.392	7.536	1.370	
3	2	8	8.222	7.127	.865	
1	0	9	7.205	7.771	.744	
2	0	9	10.964	10.050	.810	
1	1	9	4.210	3.356	3.998*	**

Vita

Robert Terrance Downs was born in Brandon, Manitoba, Canada on Thanksgiving Day, 14 October 1955. After having worked in the heavy construction trade as a surveyor for ten years, he received a Bachelor of Science degree in mathematics from the University of British Columbia, Vancouver, British Columbia in 1986. He received a Master of Science degree in the geological sciences from Virginia Polytechnic Institute and State University, Blacksburg, Virginia, in 1989. In 1991 he married his lovely wife, Dori.